PAPER

Experimental and computational analysis of supramolecular motifs involving C_{sp^2}(aromatic)–F and CF_3 groups in organic solids†

Piyush Panini,[a] Rajesh G. Gonnade[b] and Deepak Chopra*[a]

A detailed experimental (SCXRD) and theoretical (PIXEL and QTAIM) investigation of the evolution of different supramolecular motifs formed *via* the presence of both $C(sp^2)/(sp^3)$–F groups in the crystal packing has been performed in a series of newly synthesized substituted benzanilides (containing ''both'' the fluorine and the trifluoromethyl group in the same molecule) along with previously reported similarly related crystal structures [*CrystEngComm*, 2008, **10**, 54–67; *CrystEngComm*, 2012, **14**, 1972–1989; *CrystEngComm*, 2013, **15**, 3711–3733]. It was observed that the highest stabilized molecular motifs primarily consist of $C(sp^2)$–H$\cdots$F–$C(sp^2)$ H-bonds in preference to $C(sp^2)$–H$\cdots$F–$C(sp^3)$ H-bonds in the crystal. The motifs involving $C(sp^2)$–H$\cdots$F–$C(sp^2)/(sp^3)$ H bonds were observed to be present over the entire distance range between 2.2 and 2.7 Å, albeit the difference in energies of stabilization involving fluorine atoms attached to sp^2 and sp^3 carbon is not significant in molecular crystals. From QTAIM analysis, the $C(sp^2)/(sp^3)$–F$\cdots$F–$C(sp^2)/(sp^3)$ interactions were observed to be a closed shell in nature and provide local stabilization, indicating the formation of bonds, similar to weak hydrogen bonds observed in crystals.

Introduction

The introduction of a fluorine atom to the carbon atom (termed as ''Organic Fluorine'') can lead to the formation of many weak interactions like C–H$\cdots$F–C hydrogen bonds,[1,2] C–F$\cdots$F–C[3,4] and C–F$\cdots\pi$[5–7] interactions and the study of these interactions involving organic fluorine is still an expanding area of research amongst the scientific community.[8] However, there has been an enduring discussion regarding the ability of organic fluorine to act as a hydrogen bond acceptor[9–18] because of its low polarizability. However, the crystal structure analysis of fluorobenzenes[12] and ribonucleic acids[13] unfasten the area of research regarding the study of interactions involving organic fluorine. Further, such interactions with the protein active site through C–F$\cdots$C=O and C–F$\cdots$H–C_α interactions have been reviewed by Diederich *et al.*[19] Since then many studies *via* inputs from crystallography, spectroscopy and theoretical calculations have established the fact that the interactions involving fluorine are

ubiquitous and can play an important role in the stabilization of the crystal packing and influence the phenomenon and properties in the solid state, one such example is polymorphism. The extensive literature on compounds related to the presence of organic fluorine has been excellently combined in reviews[8,20–22] and a book chapter.[23] It was initially postulated that the weak interactions involving fluorine like C–H$\cdots$F–C hydrogen bonds are only significant in the absence of any other strong intermolecular forces.[24] The analysis of the nature of fluorine interactions on many molecules has been performed, wherein the possibility of the formation of strong hydrogen bonds was eliminated. Amongst these, benzene,[12,18] naphthalene, anthracene and phenanthrene,[16] isoquinolines,[24,25] trifluoroacetophenones,[26] N-phenylmaleimides and corresponding phthalimides,[27] benzonitriles,[28] pyridines,[29] azobenzenes,[30] N-benzylideneanilines,[31,32] toluene,[33] and N-methyl-N-phenylbenzamides[34] are a few examples to be mentioned. There is no sufficient literature on the study of these intermolecular interactions in molecules wherein strong intermolecular forces are present.[20] However, fluorinated N-(2-chloropyridin-4-yl)-N'-phenylureas,[35] fluoro-N-(pyridyl)-benzamides,[36] fluorine-substituted benzoic acid,[37] and fluorine-substituted benzimidazoles[38] are a few examples wherein the evaluation of interactions involving fluorine was realized in the presence of a strong hydrogen bond. Keeping in mind the above-mentioned points, improvements aimed towards the understanding of the nature, capability and energetics of interactions

[a] *Crystallography and Crystal Chemistry Laboratory, Department of Chemistry, Indian Institute of Science Education and Research Bhopal, Madhya Pradesh, India-462066. E-mail: dchopra@iiserb.ac.in; Fax: +91-0755-6692370*

[b] *Center for Materials Characterization (CMC), CSIR-National Chemical Laboratory, Pune-411008, India*

involving organic fluorine (in particular C–H···F and C–F···F–C interactions) in the presence of a strong hydrogen bond have been undertaken by our research in the past few years.[17,39–41] Our main goal was (i) a systematic exploration of the participation of the fluorine atom in different intermolecular interactions, (ii) robustness of the interaction (*i.e.* how often they are present) in the formation of different supramolecular motifs, (iii) the role of hybridization of the C-atom to which fluorine is attached and finally (iv) the calculation of stabilization energy and topological parameters such as the electron densities (ρ), Laplacian ($\nabla^2\rho$), local potential energy (V_b), and kinetic potential energy (G_b) at the bond critical point by quantum theory of atoms in molecules (QTAIM).[42] In this regard, a large library of molecules containing the organic fluorine group have been synthesized, crystallized and investigated for different intermolecular interactions involving organic fluorine. The systems were designed such that they have only one strong donor and acceptor (the amide group –NH–C=O– in our studies) atom, which connects at least one phenyl ring wherein the position of the fluorine (connected to the C-atom) of different hybridization, [C(sp^2)–F and –C(sp^3)–F$_3$ groups] may vary, keeping the main molecular connectivity invariant. Hence, different molecules, namely fluorine substituted benzanilides,[17] fluorine and –CF$_3$ substituted *N*-phenylacetamides and *N*-methylbenzamides,[39] and –CF$_3$ substituted benzanilides have been studied.[40] The purpose of selecting the CF$_3$ group is as follows: (i) the –CF$_3$ group being strongly electron-withdrawing in nature increases the acidity of hydrogen atoms in its vicinity, (ii) better H-bond acceptor abilities of C(sp^3)–F can be exploited, (iii) in addition to C–H···F–C hydrogen bonds, the propensity of the formation of other interactions namely C–F···F–C and C–F···π is now increased and (iv) in addition to all the above-mentioned points, a comparative study of the role of hybridization of the C-atom to which fluorine is attached can be achieved in the crystal.

Therefore, we have synthesized a library of substituted benzanilides (eighteen in number) containing both the fluorine and trifluoromethyl group on the same molecule (Scheme 1).

Initial investigations into two molecules in this series, namely *N*-(4-fluorophenyl)-3-(trifluoromethyl)benzamide and 4-fluoro-*N*-[3-(trifluoromethyl)phenyl]benzamide, demonstrated the existence of short H-bonds with organic fluorine in the presence of strong N–H···O=C H-bonds.[41] The nature of these interactions was tested with criteria for H-bonds proposed recently by IUPAC[43] and has also been analyzed using the PIXEL method[44–47] and the QTAIM approach.[42] It is now well established that the C–H···F interactions at short distances are indeed a "true H-bond" and these are not the consequence of crystal packing. In this current work, along with the detailed crystal packing analysis of the remaining newly synthesized compound in this series, our main focus will be on the (i) identification of different robust or reoccurring motifs formed by the interactions involving organic fluorine in the crystal, (ii) investigations of these in terms of their nature, energetics and topological properties using the PIXEL method and the QTAIM approach and (iii) the comparative study on the role of hybridization[48] of the C-atom to which fluorine is attached, based on the inputs obtained from current and previous series of molecules[17,39,40] having a similar molecular framework.

Experimental section

All the compounds were synthesized by the procedure that is already reported in the literature.[40] Scheme 1 describes the general route for the synthesis of all the 18 compounds and their corresponding nomenclature code used in this paper. All the synthesized compounds were characterized by FTIR [Fig. S1(a–p)], and ^{1}H NMR [Fig. S2(a–p)] (Section S1, ESI†). Melting points were recorded using a DSC [Fig. S3(a–p), ESI†] on the pure powder compounds. Powder X-ray diffraction (PXRD) data were recorded for all the solid compounds and then compared with their calculated PXRD patterns [Fig. S4(a–p), ESI†]. In order to ensure the phase purity, a profile fitting refinement (Section S2, ESI†) was performed using a JANA2000.[49]
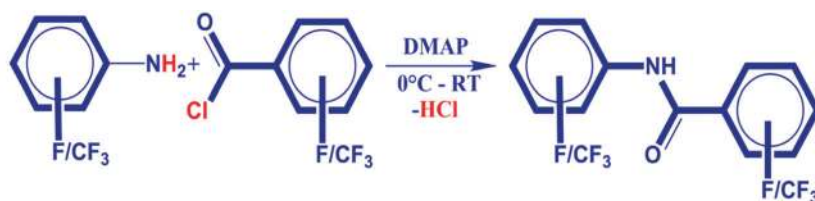
entry	A	B	Code	entry	A	B	Code	entry	A	B	Code
1	*o*-F	*o*-CF$_3$	1F1T	7	*o*-F	*p*-CF$_3$	1F3T^a	13	*o*-CF$_3$	*m*-F	1T2F
2	*m*-F	*o*-CF$_3$	2F1T	8	*m*-F	*p*-CF$_3$	2F3T	14	*m*-CF$_3$	*m*-F	2T2F
3	*p*-F	*o*-CF$_3$	3F1T^a	9	*p*-F	*p*-CF$_3$	3F3T	15	*p*-CF$_3$	*m*-F	3T2F^a
4	*o*-F	*m*-CF$_3$	1F2T	10	*o*-CF$_3$	*o*-F	1T1F^a	16	*o*-CF$_3$	*p*-F	1T3F
5	*m*-F	*m*-CF$_3$	2F2T	11	*m*-CF$_3$	*o*-F	2T1F^c	17	*m*-CF$_3$	*p*-F	2T3F^b
6	*p*-F	*m*-CF$_3$	3F2T^b	12	*p*-CF$_3$	*o*-F	3T1F	18	*p*-CF$_3$	*p*-F	3T3F

^{a} Single crystal suitable for SCXRD could not be obtained; ^{b} Reported in ref [41] ; ^{c} observed also as its hydrate (code: 2T1F_w).

Scheme 1 Synthetic scheme of all the compounds along with their nomenclature plan used in this manuscript are presented.

In the case of **1F2T**, **2F3T**, **2T1F** and **3T1F**, high values of the profile fitting parameters (R_p, R_{wp}) were observed, which may indicate the possibility of the presence of more than one phase in the bulk powder.

The details of all the crystallization experiments of all the solid compounds from different solvents and solvent mixtures are presented in the ESI† (Table S1).

Data collection, structure solution and refinement

Single crystal X-ray diffraction data were collected on a Bruker AXS SMART APEX II CCD diffractometer at 100 K. All the data were collected at 100(2) K. All the crystal structures were solved by direct methods using SIR 92[50] and refined using the full matrix least-squares method using SHELXL2013[51] present in the program suite WinGX.[52] The non-hydrogen atoms were refined anisotropically and the hydrogen atoms bonded to C and N atoms were positioned geometrically and refined using a riding model with $U_{iso}(H) = 1.2U_{eq}$ [C(sp^2)]. The disorder associated with the CF$_3$ group (in the case of compounds **2F2T** and **2T1F_w**) and the positional disorder of the F-atom (in the case of compounds **1F1T**, **2F1T**, **2F2T**, **2T1F**, **2T1F_w** and **2T2F**) were modeled with PART command in SHELXL 2013 at two independent orientations (the major component was labeled 'A') (Fig. S5, ESI†). Molecular and packing diagrams were generated using Mercury software.[53] Table S2 (ESI†) lists all the crystallographic and refinement data. ORTEPs of all compounds are presented in Fig. S5(a–m) in the ESI.†

Computational tools and theoretical calculations

The PIXEL method [in the CLP computer program package (version 10.2.2012)] has been used for the interaction energy of the selected molecular pairs, extracted from the crystal packing and related by the corresponding symmetry element as mentioned in our previous work.[41] In the method, the total interaction energy is partitioned into their Coulombic (E_{coub}), polarization (E_{pol}), dispersion (E_{disp}) and repulsion (E_{rep}) contributions. In the case of disordered molecules, the molecular conformation with the maximum population was considered for the calculations. The PIXEL method was observed to provide better and useful insights into the nature of different types of intermolecular interactions present in the different molecular pairs/motifs.[54–57] The PIXEL interaction energy was further compared with the interaction energies obtained from theoretical calculations at the DFT+Disp/B97D[58,59] level at the higher aug-cc-pVTZ basis set using TURBOMOLE.[60] The hydrogen atoms were moved to neutron values (1.083 Å for C–H) before the calculations. The basis set superposition error (BSSE) for the interaction energies was corrected by using the counterpoise method.[61] Table S3 (ESI†) (divided into two parts: S3a and b, separately for C–F···F–C in Table S3b, ESI†) lists the selected intermolecular interactions (in the decreasing order of their stabilization energy) in different motifs along with their interaction energies (I.E.) of the motifs. In the case of highly disordered compounds **2T1F_w** [having the rotational disorder associated with the CF$_3$ group and the positional disorder of the fluorine atom at the phenyl ring along with the presence of

half molecule of water in the asymmetric unit, Fig. S5(h), ESI†], PIXEL calculations have not been performed. Instead, BSSE corrected interaction energies for the selected dimers were calculated at the DFT+Disp/B97D level using the aug-cc-pVTZ basis set (Table S5, ESI†).

### Analysis of topological parameters (QTAIM calculations)

Topological calculations on the selected dimers at the crystal geometry were performed using the same procedure as mentioned previously[41] using AIMALL (version 13.05.06).[62] The selected topological parameters like electron densities (ρ_c), Laplacian ($\nabla^2\rho_c$), local potential energy (V_b), and kinetic energy density (G_b) at the bond critical points (BCPs) were calculated. The dissociation energies for different intermolecular interactions were also estimated through the following two empirical approaches: (i) D.E.^{V}(int) = $-0.5V_b$ (in atomic units)[63] and (ii) D.E.^{G}(int) = $0.429G_b$ (in atomic units),[64,65] where D.E.(int) is the dissociation energy of the interaction. Interaction energy (I.E.) = $-$D.E. V_b and G_b are the local potential and kinetic energy density at the bond critical points (BCPs), respectively. The results of the topological analysis on different molecular pairs are presented in Section S4 (Tables S4 and S5) in the ESI.† Topological parameters of the selected C–H···F and C–F···F–C interactions in different motifs along with their dissociation energy are presented in Table S4b (ESI†). Compounds having disorder associated with the CF$_3$ group or fluorine (positional disorder) were not considered for the calculations except for **1F1T** and **2T2F** wherein the positional disorder of fluorine with an occupancy ratio at the two positions was observed to be 0.875(2):0.125(2) and 0.944(3):0.056(3) respectively. In these cases, the molecular conformation with the maximum population was considered for the calculations.

Results and discussion

(1) *N*-(2-Fluorophenyl)-2-(trifluoromethyl)benzamide (1F1T)

Compound **1F1T** crystallizes in the orthorhombic non-centrosymmetric space group $Pna2_1$ with $Z = 4$. A strong N–H···O=C H-bond along with a weak C–H···π hydrogen bond (motif **I**, -12.7 kcal mol^{-1}, Table S3a, ESI†) was observed to connect the molecules along the crystallographic *a*-axis in the formation of the molecular chain [Fig. 1(a)]. Such chains are interconnected *via* a weak C–H···F–C$_{sp^3}$ hydrogen bond (motif **V**, -1.5 kcal mol^{-1}). Furthermore, there exists the formation of the herringbone pattern observed down the *bc* plane in the crystal packing, stabilized *via* the presence of motif **II** (involving C–H···O and C–H···F–C$_{sp^2}$ hydrogen bonds, -6.2 kcal mol^{-1}) and weak C–H···F–C$_{sp^3}$ hydrogen bonds in motif **IV** (-1.9 kcal mol^{-1}). Weak C–H···O=C and C–H···F–C$_{sp^3}$ hydrogen bonds were found to stabilize the crystal packing (motif **III**, -4.8 kcal mol^{-1}) in the generation of a molecular chain [Fig. 1(c)]. It is to be noted that the stabilization energy for a C–H···F hydrogen bond was reported to be ~ -0.40 kcal mol^{-1} (-1.6 kJ mol^{-1}) by *ab initio* theoretical calculation for the neutral molecule by D'Oria and Novoa.[66]
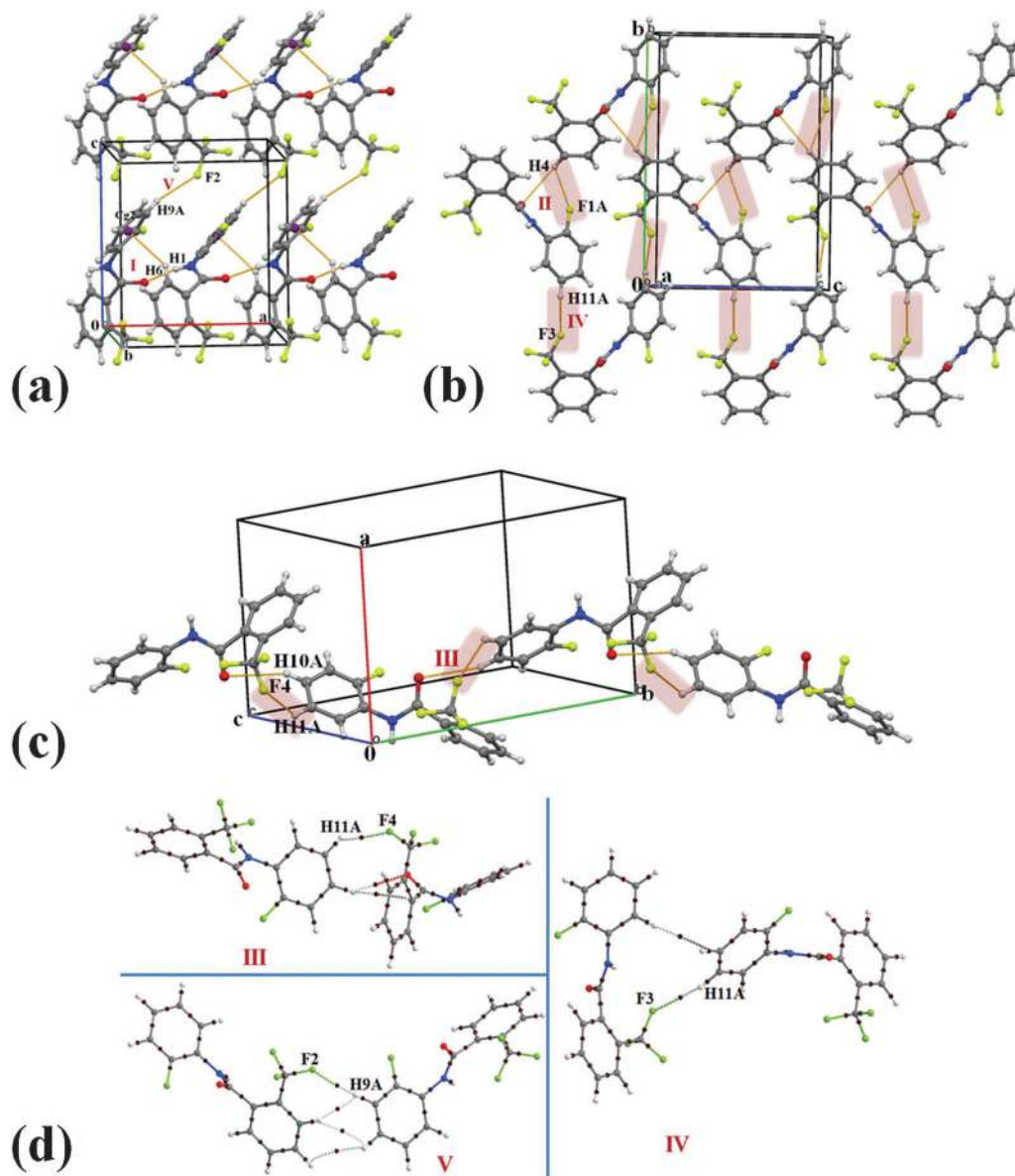
Fig. 1 (a) Packing of molecules in **1F1T** *via* the network of strong N–H···O=C, weak C–H···π and C–H···F–C_{sp^3} hydrogen bonds. The Roman numbers in red (in this and also subsequent diagrams) indicate the molecular motifs presented in Table S3 (ESI†). (b) Formation of the herringbone layer of molecules down the *bc* plane with the utilization of weak C–H···O, C–H···F–C_{sp^2} and C–H···F–C_{sp^3} hydrogen bonds in **1F1T**. (c) Formation of the molecular chain in **1F1T** *via* weak C–H···O and C–H···F–C_{sp^3} hydrogen bonds. (d) Selected molecular motifs (denoted with Roman numbers from Table S4, ESI†) in **1F1T**, showing different intermolecular interactions. The brown small spheres represent bond critical points (BCPs) on the bond path.

The presence of weak C–H···F–C hydrogen bonds in the motifs **III**, **IV** and **V** was characterized topologically by using the QTAIM approach. There was the presence of (3, −1) bond critical points (BCPs) recognized for these interactions (Table S4b, ESI†) along with other related interactions present in the respective motifs [Fig. 1(d)].

(2) *N*-(3-Fluorophenyl)-2-(trifluoromethyl)benzamide (2F1T)

Compound **2F1T** crystallizes in the monoclinic centrosymmetric space group $P2_1/c$ with three molecules in the asymmetric unit ($Z' = 3$) (Fig. 2). Two (molecule **2** and **3**) out of three molecules in the asymmetric unit observed in the formation of the most

stabilized molecular motif **I** (−13.3 kcal mol^{-1}) involved strong N–H···O=C, weak C–H···π and C–H···F–C_{sp^3} hydrogen bonds along with π···π interactions. Selected molecular pairs, which contribute towards the stabilization of the crystal packing in **2F1T**, are presented in Fig. 2(c) along with their interaction energies (I.E.). The three most stabilized molecule motifs **I**, **II** (−13.1 kcal mol^{-1}) and **III** (−12.2 kcal mol^{-1}), consisting of strong N–H···O=C hydrogen bonds along with other weak interactions (Table S3a, ESI†), were observed to be involved in the formation of a molecular chain along the crystallographic *a*-axis in the crystal packing [Fig. 2(a) and (b)]. Such chains were observed to be connected with the utilization of motifs **IV**,
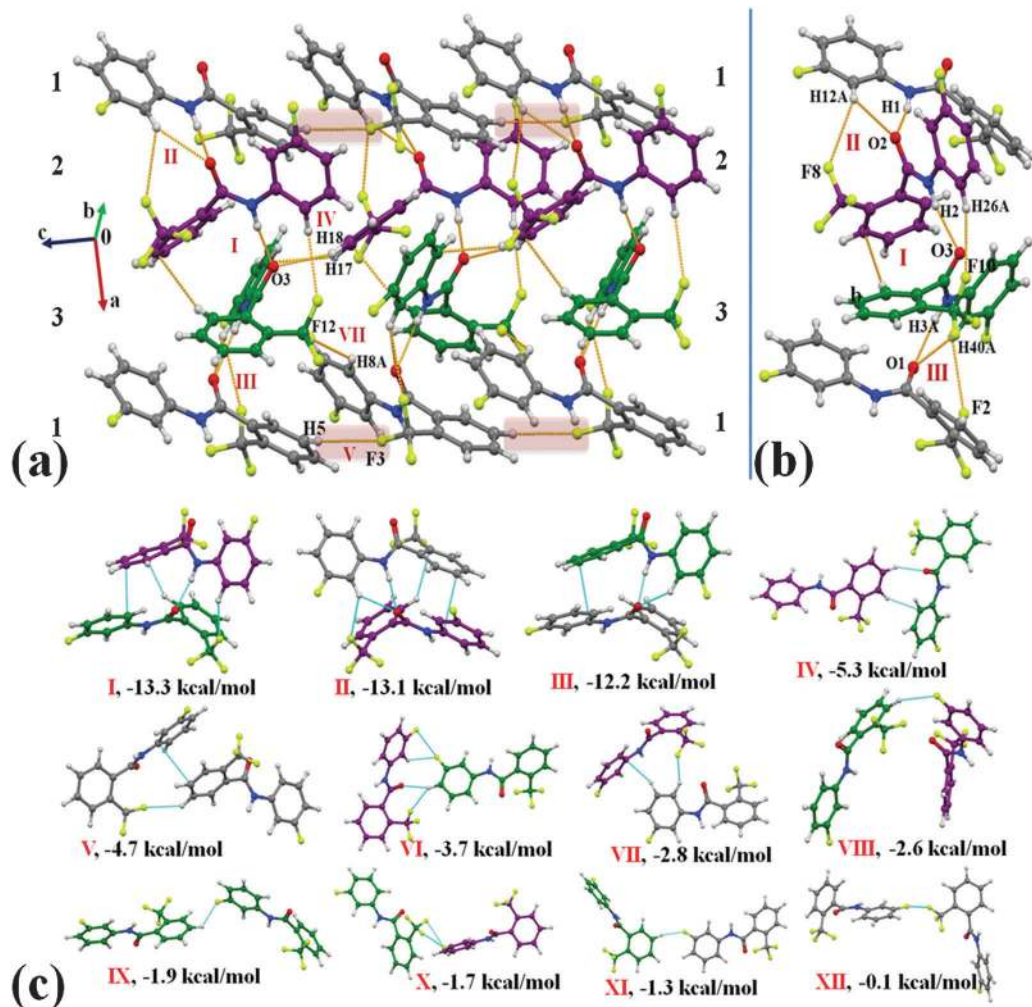
Fig. 2 (a) Packing of molecules in **2F1T** *via* the network of strong N–H···O=C, weak C–H···π and C–H···F–C$_{sp^3}$ hydrogen bonds. (b) Clear depiction of the ...123... molecular chain along the crystallographic *a*-axis. Different color codes of carbon atoms indicate the presence of three molecules in the asymmetric unit. Grey: molecule 1, purple: molecule 2 and green: molecule 3. (c) Selected molecular pairs extracted from the crystal packing of **2F1T** along with their interaction energies (Table S3, ESI†).

V and **VII** in the crystal packing [Fig. 2(a)]. The motif **IV** (I.E. = −5.3 kcal mol⁻¹) consists of short C–H···O=C (2.39 Å/149°) and C–H···π (2.68 Å/141°) hydrogen bonds while the motif **V** (−4.7 kcal mol⁻¹) involves the presence of weak C–H···F–C$_{sp^3}$ hydrogen bonds [Fig. 2(a)] along with π···π interactions. A short C–H···F–C$_{sp^3}$ (2.39 Å/127°) and a weak C–H···π (2.86 Å/155°) hydrogen bond were recognized to connect the molecules in motif **VII**. Moreover, the packing of molecules in **2F1T** are also stabilized by the presence of weak C–H···F–C$_{sp^2}$ hydrogen bonds in the motifs **VIII**, **IX** and **XI** with the stabilization energy ranging from −1.3 to −2.6 kcal mol⁻¹ [Table S3, ESI† and Fig. 2(c)]. It is to be noted that the motif **X**, involves the presence of bifurcated C$_{sp^2}$–F···F–C$_{sp^3}$ interactions [type I (2.883 Å, 110°, 94°) and other a "near" type II (3.133 Å, 152°, 83°) contact], provides stabilization towards the crystal packing with an interaction energy of 1.7 kcal mol⁻¹, the nature being primarily of dispersive origin. A very recent charge density analysis has revealed the polarization of the electron density on the fluorine atoms on the trifluoromethyl group, which facilitate the

formation of type II C–F···F–C contacts in the crystal.[67] Furthermore, a very short type I C$_{sp^2}$–F···F–C$_{sp^3}$ interaction [2.736 Å, 146°, 149°, motif **XII**] was observed in the crystal packing, providing almost negligible stabilization [0.1 kcal mol⁻¹] [Fig. 2(c)]. This stabilization energy is similar to the value reported in a recent analysis by *ab initio* calculations on all the unique dimers, extracted from the crystal structure of CF₄, C₂F₄ and C₆F₆ by Osuna *et al.*[68]

(3) N-(2-Fluorophenyl)-3-(trifluoromethyl)benzamide (1F2T)

Compound **1F2T** crystallizes in the monoclinic centrosymmetric space group with *Z* = 4. Fig. 3(a) depicts the packing of molecules in **1F2T** in all the three directions with the utilization of different molecular motifs **I** to **VIII** (Table S2, ESI†). The highest stabilized molecular motif **I** (I.E. = −11.8 kcal mol⁻¹) consists of strong N–H···O=C, a short and directional C–H···F–C$_{sp^2}$ (2.47 Å, 168°) and a short C–H···π (2.66 Å, 158°) hydrogen bond along with C–F···π interactions. The motif **I** along with motif **III** [I.E. = −4.8 kcal mol⁻¹; consists of a short
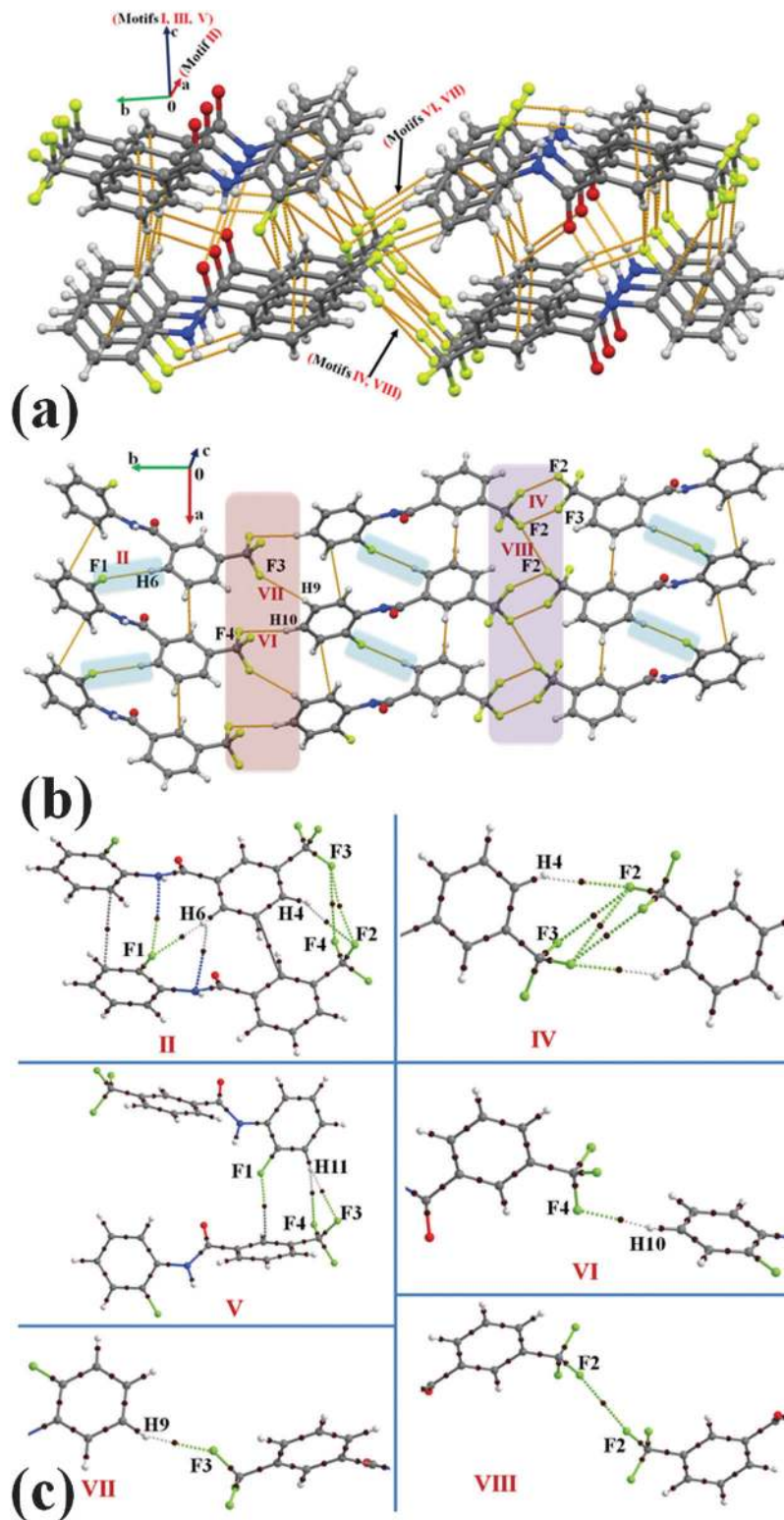
Fig. 3 (a) Packing of the molecules down the *bc* crystallographic plane in **1F2T** *via* the network of strong N–H···O═C, weak C–H···π, C–H···F–C$_{sp^2}$ and C–H···F–C$_{sp^3}$ hydrogen bonds along with π···π, C$_{sp^3}$–F···π and C$_{sp^3}$–F···F–C$_{sp^3}$ interactions. (b) Part of the crystal packing in **1F2T** down the *ab* plane, displaying the presence of weak C–H···F–C$_{sp^2}$ and C–H···F–C$_{sp^3}$ hydrogen bonds along with π···π (off set) and C$_{sp^3}$–F···F–C$_{sp^3}$ interactions. (c) Selected molecular motifs (denoted with Roman numbers from Table S4, ESI†) in **1F2T**, showing different intermolecular interactions. The small brown spheres represent bond critical points (BCPs) on the bond path. Only the interacting part of the motifs is shown in case of **IV**, **VI–VIII**.

C–H$\cdots\pi$ (2.61 Å, 159°) and C–H$\cdots$O=C hydrogen bond] and motif **V** (I.E. = −1.9 kcal mol^{-1}; involves a bifurcated C–H$\cdots$F–C$_{sp^3}$ along with the presence of C–F$\cdots\pi$ interactions) were observed to pack the molecules along the c-axis with the utilization of c-glide perpendicular to b-axis. A short and directional C–H$\cdots$F–C$_{sp^2}$ (2.45 Å, 168°) hydrogen bond along with the two $\pi\cdots\pi$ interactions in the motif **II** (−6.4 kcal mol^{-1}) was observed to connect the molecules along the crystallographic a-axis.
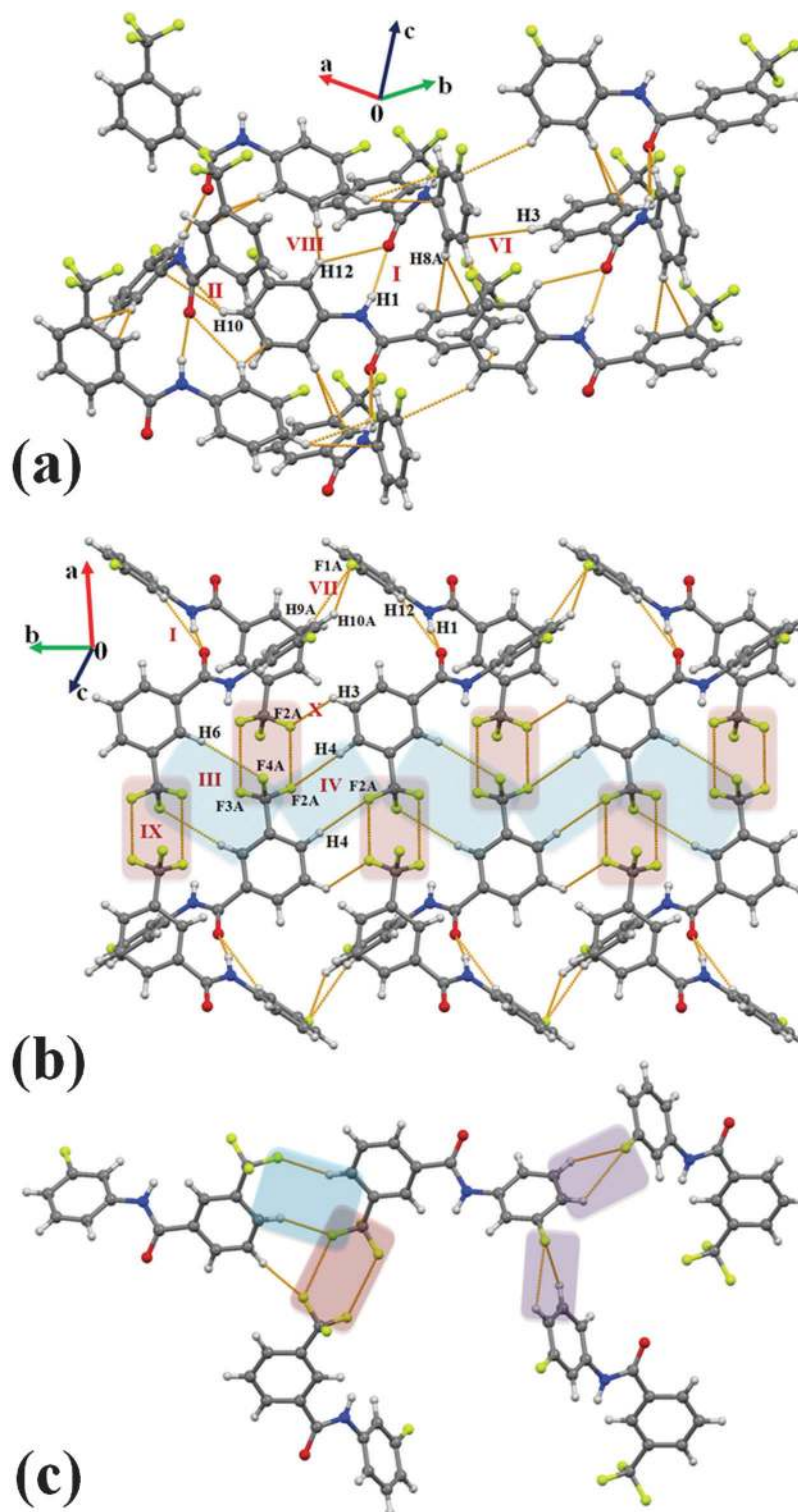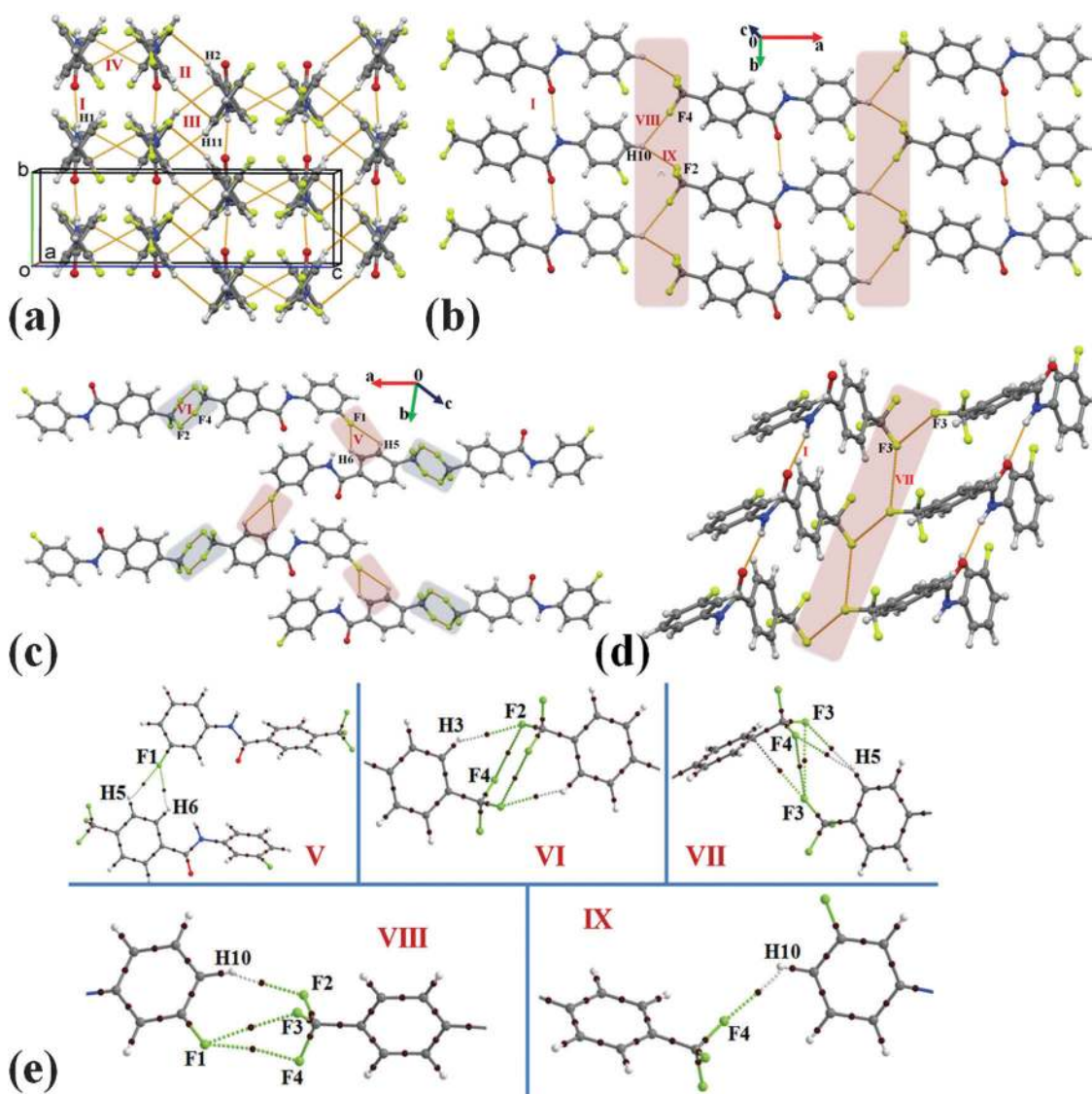

Fig. 4 (a) Packing of molecules in **2F2T** *via* the network of strong N–H$\cdots$O=C, and weak C–H$\cdots$O, C–H$\cdots\pi$ hydrogen bonds. (b) Packing of molecules in **2F2T**, displaying the network of strong N–H$\cdots$O=C, weak C–H$\cdots$O, C–H$\cdots$F–C$_{sp^2}$ and C–H$\cdots$F–C$_{sp^3}$ hydrogen bonds along with C$_{sp^3}$–F$\cdots$F–C$_{sp^3}$ interactions. (c) Part of crystal packing in **2F2T**, depicting the presence of different motifs involving fluorine interactions.

The molecular chains, formed along the a-axis, with the utilization of motif II [Fig. 3(b)], were observed to be connected *via* motifs **IV**, **VI** to **VIII** in the generation of a molecular layer down the *ab* plane. Amongst these, motif **VI** (-1.5 kcal mol^{-1}) and **VII** (-1.1 kcal mol^{-1}) were found to consist of a short C–H$\cdots$F–C$_{sp^3}$ (2.47 Å, 161°; 2.57 Å, 139°) hydrogen bond while the motif **IV** (I.E. = -2.0 kcal mol^{-1}) involves dimeric C$_{sp^3}$–F$\cdots$F–C$_{sp^3}$ interaction and a weakly stabilized (-0.2 kcal mol^{-1}) motif **VIII** consists of type I C$_{sp^3}$–F$\cdots$F–C$_{sp^3}$ (2.942 Å, 158°, 158°) interactions. Further, QTAIM calculations reveal the presence of a (3, -1) BCP for all C–H$\cdots$F and C–F$\cdots$F–C interactions [Fig. 3(c)].

(4) *N*-(3-Fluorophenyl)-3-(trifluoromethyl)benzamide (2F2T)

Compound **2F2T** crystallizes in the orthorhombic centro-symmetric space group *Pbcn* with $Z = 8$. The most stabilized molecular motif **I** (I.E. = -12.1 kcal mol^{-1}) consists of strong N–H$\cdots$O═C hydrogen bonds supported by weak C–H$\cdots$O and C–H$\cdots\pi$ hydrogen bonds. A molecular chain, formed *via* motif **I** utilizing *c*-glide, was observed to connect *via* the weak C–H$\cdots\pi$ hydrogen bonds recognized in the motif **II** (-4.2 kcal mol^{-1}), **VI** (-2.1 kcal mol^{-1}), **VIII** (-1.6 kcal mol^{-1}) [Fig. 4(a)]. Furthermore, the packing of molecules in **2F2T** was stabilized by the formation of motifs **III** (-3.0 kcal mol^{-1}) and **IV** (-2.4 kcal mol^{-1}), comprising of dimeric weak C–H$\cdots$F–C$_{sp^3}$ hydrogen bonds.

Fig. 5 (a) Formation of a molecular layer down the *bc* crystallographic plane with the utilization of strong N–H$\cdots$O═C, weak C–H$\cdots\pi$ hydrogen bonds and $\pi\cdots\pi$ interactions in **2F3T**. (b) Packing of molecules down the *ab* plane *via* the networks of strong N–H$\cdots$O═C and weak C–H$\cdots$F–C$_{sp^3}$ hydrogen bonds in **2F3T**. (c) Part of the crystal packing in **2F3T**, displaying the formation of bifurcated weak C–H$\cdots$F–C$_{sp^2}$ hydrogen bonds and dimeric C$_{sp^3}$–F$\cdots$F–C$_{sp^3}$ interactions. (d) Part of the crystal packing **2F3T** showing the presence of C$_{sp^3}$–F$\cdots$F–C$_{sp^3}$ interactions forming a chain motif along with a strong N–H$\cdots$O═C hydrogen bond. (e) Selected molecular motifs (Table S4, ESI†) in **2F3T**, showing different intermolecular interactions. The small brown spheres represent bond critical points (BCPs) on the bond path. Only the interacting part of the motif was shown in the case of **VI–IX**.

It is of interest to note that a short and directional C_{sp^3}–F$\cdots\pi$ [3.134 Å, 150°, Table S3, ESI†] interaction, utilizing 2-fold rotation parallel to the *b*-axis, provided (motif **V**) stabilization to the crystal packing [2.3 kcal mol^{-1}] with dispersion being a major contributor. Moreover, bifurcated weak C–H$\cdots$F–C_{sp^2} hydrogen bonds (motif **VII**, −1.7 kcal mol^{-1}) were realized in the formation of a molecular chain, utilizing a *c*-glide plane perpendicular to the *b*-axis. Such chains were connected with the presence of motif **IX** (−0.2 kcal mol^{-1}), possessing a pair of weak type I C_{sp^3}–F$\cdots$F–C_{sp^3} interactions including the one at a short distance (2.873 Å, 122°, 122°) [Fig. 4(b)]. It was also noticed that the two sides of the phenyl ring, substituted with

the fluorine and –CF$_3$ group, were observed in the formation of different supramolecular motifs in the crystal packing [Fig. 4(c)].

(5) *N*-(3-Fluorophenyl)-4-(trifluoromethyl)benzamide (2F3T)

Compound **2F3T** was found to crystallize in the monoclinic centrosymmetric space group *C*2/*c* with *Z* = 8. The strong N–H$\cdots$O$=$C hydrogen bond along with the weak C–H$\cdots$O$=$C hydrogen bond and $\pi\cdots\pi$ interactions (motif **I**, −12.3 kcal mol^{-1}) were observed to engage in the formation of molecular chains along the crystallographic *b*-axis. Such a chain is connected by the utilization of weak C–H$\cdots\pi$ hydrogen bonds and $\pi\cdots\pi$ interactions in the formation of a molecular layer down the
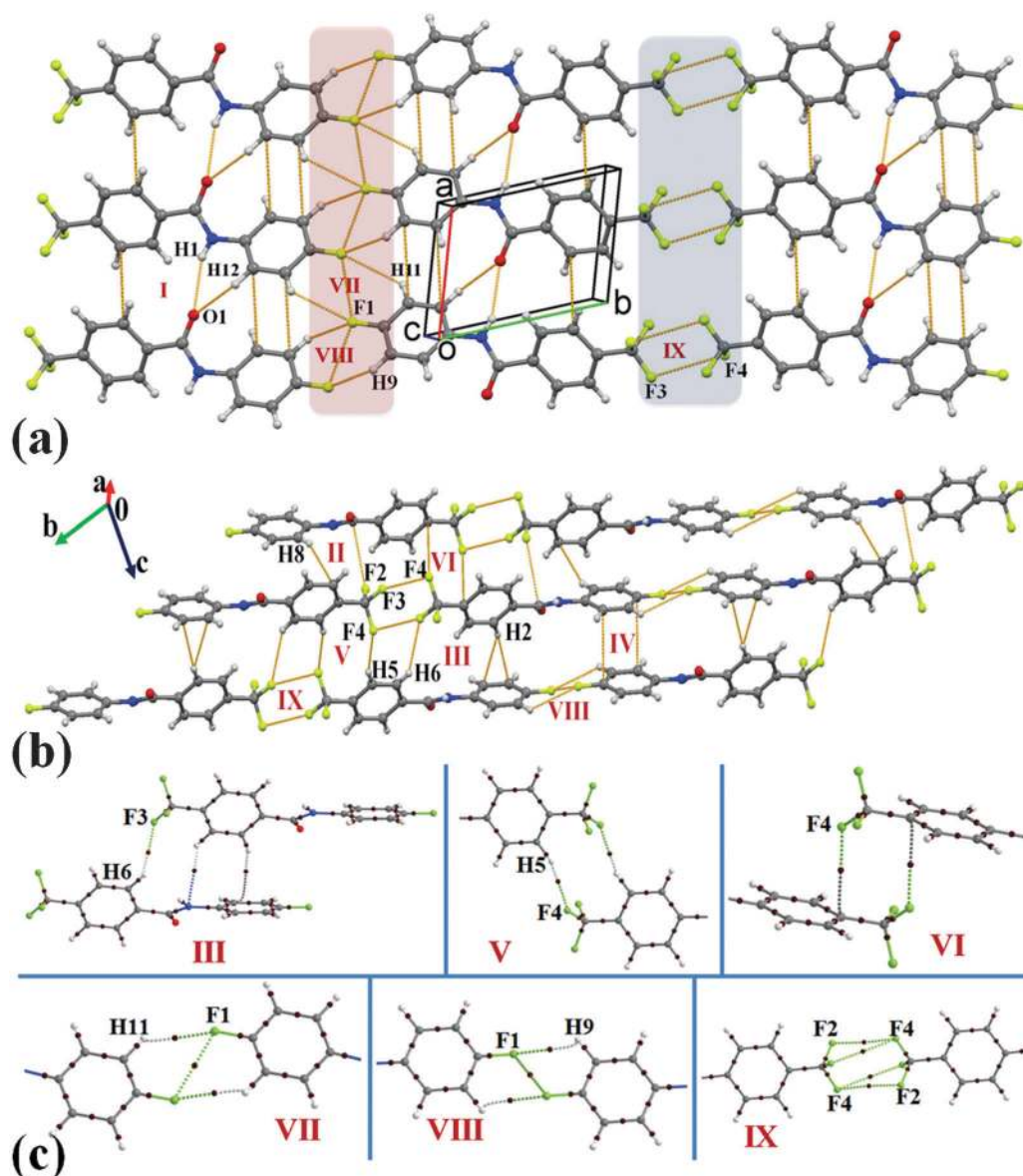

Fig. 6 (a) Packing of molecules in **3F3T** down the *ab* crystallographic plane with the utilization of strong N–H$\cdots$O$=$C, weak C–H$\cdots$O$=$C, C–H$\cdots$F–C_{sp^2} hydrogen bonds along with C_{sp^2}–F$\cdots$F–C_{sp^2}, C_{sp^3}–F$\cdots$F–C_{sp^3} and $\pi\cdots\pi$ interactions. (b) Packing of molecules in **3F3T** down the *bc* crystallographic plane *via* weak C–H$\cdots$F–C_{sp^2}, C–H$\cdots$F–C_{sp^3} and C–H$\cdots\pi$ hydrogen bonds along with C_{sp^2}–F$\cdots$F–C_{sp^2}, C_{sp^3}–F$\cdots$F–C_{sp^3}, C_{sp^3}–F$\cdots$O$=$C, C_{sp^3}–F$\cdots\pi$ and $\pi\cdots\pi$ interactions. (c) Selected molecular motifs (Table S4, ESI†) in **3F3T**, showing different intermolecular interactions. The small brown spheres represent bond critical points (BCPs) on the bond path. Only the interacting part of the motif is shown in the case of **III**, **V–VII**, **IX** and **X**.

bc plane [Fig. 5(a)], involved in the next three stabilized motifs **II** (−7.6 kcal mol⁻¹), **III** (−7.4 kcal mol⁻¹) and **IV** (−6.1 kcal mol⁻¹). The packing of molecules down the *bc* plane [Fig. 5(b)] was detected as the formation of a molecular sheet with the utilization of bifurcated weak and short C–H$\cdots$F–C$_{sp^3}$ hydrogen bonds [2.55 Å, 145° (motif **VIII**, −1.3 kcal mol⁻¹); 2.55 Å, 125° (motif **IX**, −1.1 kcal mol⁻¹)], along the *b*-axis. Furthermore, the crystal packing of **2F3T** was also observed to be stabilized by the formation

of similarly stabilized molecular motifs **V** (−2.2 kcal mol⁻¹) and **VI** (−2.1 kcal mol⁻¹) [Fig. 5(c)]. The motif **V** consists of bifurcated weak C–H$\cdots$F–C$_{sp^2}$ hydrogen bonds while the motif **VI** involves in the formation of dimeric C$_{sp^3}$–F$\cdots$F–C$_{sp^3}$ interactions. In addition, a type II C$_{sp^3}$–F$\cdots$F–C$_{sp^3}$ interaction (motif **VII**, −1.9 kcal mol⁻¹) was also observed to form a chain, utilizing the 2₁ screw axis along the crystallographic *b*-axis in the crystal packing [Fig. 5(d)]. The selected motifs, containing weak
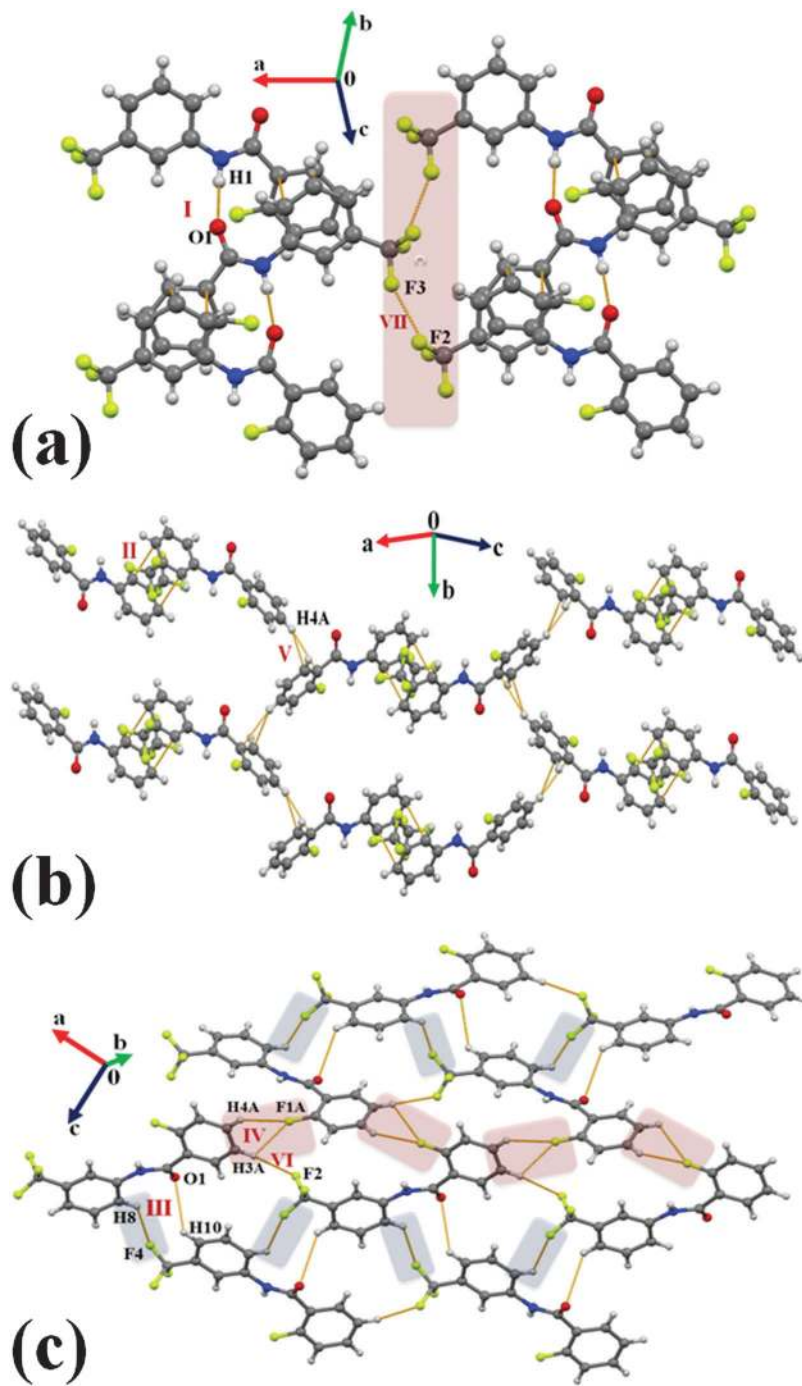

Fig. 7 (a) Packing of molecules in **2T1F** *via* strong N–H$\cdots$O=C hydrogen bonds along with C$_{sp^3}$–F$\cdots$F–C$_{sp^3}$ and π$\cdots$π interactions. (b) Packing of molecules in **2T1F** *via* the network of weak C–H$\cdots$π hydrogen bonds and π$\cdots$π interactions. (c) Formation of a molecular layer in **2T1F** down the *ac* crystallographic plane with the utilization of weak C–H$\cdots$O, C–H$\cdots$F–C$_{sp^2}$ and C–H$\cdots$F–C$_{sp^3}$ hydrogen bonds.

C–H···F and C_{sp^3}–F···F–C_{sp^3} interactions, were characterized by the QTAIM theory and the presence of (3, −1) BCPs was observed on the bond path of these interactions [Fig. 5(e) and Table S5, ESI†].

(6) N-(4-Fluorophenyl)-4-(trifluoromethyl)benzamide (3F3T)

Compound **3F3T** crystallizes in the triclinic centrosymmetric space group $P\bar{1}$ with $Z = 2$. As expected, the most stabilized molecular motif **I** (−11.7 kcal mol^{-1}) was noticed to involve strong N–H···O=C hydrogen bonds along with weak C–H···O=C hydrogen bonds and π···π interactions. The motif **I** was found to be involved in the formation of a molecular chain along the crystallographic a-axis. Such chains were interlinked via dimeric weak C–H···F–C_{sp^2} hydrogen bonds [motif **VII** (−1.4 kcal mol^{-1}) and **VIII** (−1.1 kcal mol^{-1})] and dimeric weak C_{sp^3}–F···F–C_{sp^3} interactions [motif **IX** (−0.7 kcal mol^{-1})] in the formation of a molecular layer down the ab plane. Further, in the molecular packing of **3F3T**, the molecular chains formed with the utilization of motifs **VIII** and **IX** were observed to be connected by the molecular motifs **II** to **VI** which consist of other weak interactions in the crystal packing [Fig. 6(b)]. The motif **II** involves the presence of a weak C–H···π hydrogen bond and a short C_{sp^3}–F···O=C (3.118 Å, 120°) interaction, the interaction energy being −6.1 kcal mol^{-1}. The motifs **III** and **IV** were noticed to provide similar stabilization towards the crystal packing (−4.7 kcal mol^{-1} and −4.0 kcal mol^{-1} respectively) but observed to involve different interactions. The motif **III** consists of weak C–H···F–C_{sp^3} and C–H···π hydrogen bonds while the weak π···π interaction was observed in motif **IV**. Moreover, a dimeric short C–H···F–C_{sp^3} (2.45 Å, 157°) contact was observed to stabilize (motif **V**, −2.8 kcal mol^{-1}) the crystal packing in **3F3T**. In addition, dimeric weak C_{sp^3}–F···π interactions (motif **VI**, −2.2 kcal mol^{-1}) were also observed to provide stabilization to the crystal packing in **3F3T**. The weak interactions involving fluorine in **3F3T** were studied with QTAIM theory and the presence of (3, −1) BCP was observed for these interactions in their corresponding molecular motifs [Fig. 6(c)].

(7) 2-Fluoro-N-(3-(trifluoromethyl)phenyl)benzamide (2T1F)

Compound **2T1F** crystallizes in the centrosymmetric orthorhombic space group $Pbca$ with $Z = 8$. A strong N–H···O=C hydrogen bond along with π···π interactions (motif **I**, −11.6 kcal mol^{-1}) was observed in the generation of a zig-zag chain with the utilization of b-glide perpendicular to the a-axis. The chains are interconnected utilizing motif **VII** which consists of the weak near type II C_{sp^3}–F···F–C_{sp^3} (2.990 Å, 108°, 154°) interactions (I.E. being −1.0 kcal mol^{-1}). The next most stabilized motif **II** (−4.5 kcal mol^{-1}), consisting of weak π···π interaction, was found to connect the molecular chain [Fig. 7(b)] generated via a 2_1-screw along the b-axis utilizing weak C–H···π hydrogen bonds (motif **V**, −2.8 kcal mol^{-1}). Furthermore, there was the formation of a herringbone pattern down the ac plane [Fig. 7(c)] observed in the crystal packing of **2T1F**, exploiting motifs **III**, **IV** and **VI**. The motif **III** (−3.0 kcal mol^{-1}) was noticed to involve weak C–H···O and C–H···F–C_{sp^3} hydrogen bonds while it was short bifurcated C–H···F–C_{sp^2} hydrogen bonds which were observed in the motif **IV**, the stabilization energy being 2.8 kcal mol^{-1}. Moreover, a weak C–H···F–C_{sp^3} hydrogen bond was recognized in the motif **VI** (−1.4 kcal mol^{-1}).

(8) 2-Fluoro-N-(3-(trifluoromethyl)phenyl)benzamide hydrate (2T1F_w)

Hydrate of the compound 2-fluoro-N-(3-(trifluoromethyl)phenyl)-benzamide hydrate (**2T1F_w**) crystallizes in the orthorhombic centrosymmetric space group $Pbcn$ with half molecule of water in the asymmetric unit (Table S2, ESI†). It has been characterized using differential scanning calorimetry (DSC), thermal gravimetry analysis (TGA) and hot stage microscopy (HSM) (Section S3 in the ESI†). The packing of the molecules in **2T1F_w** was observed to be stabilized by the solvent molecule with the formation of strong hydrogen bonds like N–H···O_{water} and O_{water}–H···O=C, noticed in motifs **I** and **II** with I.E. being −5.04 kcal mol^{-1} and −5.63 kcal mol^{-1} respectively [Table S3c, ESI,† and Fig. 8(a)]. A stacked motif **III** along the a-axis (utilizing a 2_1-screw), consisting of two weak C–H···F–C_{sp^3} hydrogen bonds along with π···π interactions, is a highly stabilized (−14.2 kcal mol^{-1}) molecular pair in the crystal packing [Fig. 8(a) and Table S3c, ESI†]. The packing of the molecules down the bc plane shows the formation of a molecular layer utilizing motifs **I**, **II**, **IV** and **V** [Fig. 8(b)]. The molecular chain
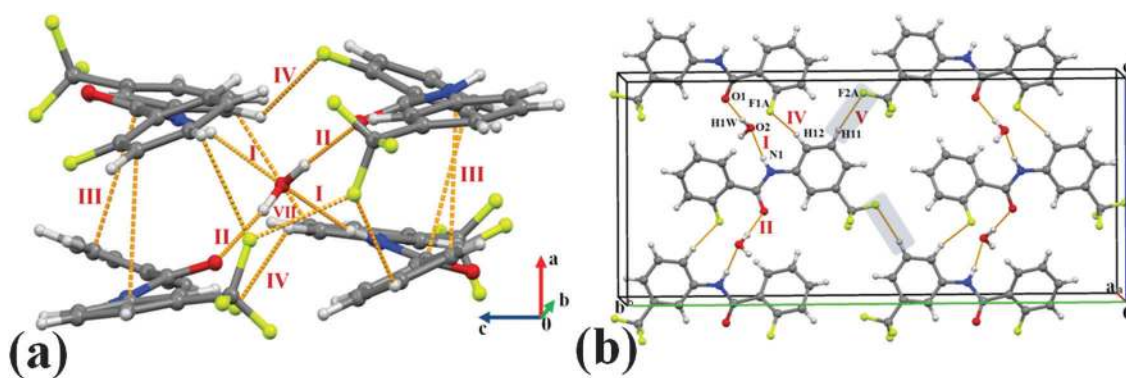

Fig. 8 (a) Part of the crystal packing in **2T1F_w** displaying the formation of strong N–H···O_{water} and O_{water}–H···O=C, and weak C–H···F–C_{sp^3} hydrogen bonds along with C_{sp^3}–F···F–C_{sp^3} and π···π interactions. (b) Packing view down the bc plane in **2T1F_w** displaying the formation of the molecular layer utilizing interactions involving the solvent along with C–H···F–C_{sp^3} hydrogen bonds.

with alternate interactions of the compound and solvent was observed to be connected with weak C–H···F–C$_{sp^3}$ hydrogen bonds (motif **V**, −1.64 kcal mol^{-1}) utilizing *c*-glide perpendicular to the *b*-axis [Fig. 8(b)]. Moreover, the presence of highly short type I C$_{sp^3}$–F···F–C$_{sp^3}$ interactions was recognized in the weakly stabilized molecular motif **VI** (−0.42 kcal mol^{-1}) and relatively destabilized motif **VII** (+1.29 kcal mol^{-1}) (Table S3c, ESI†). It is to be noted here that the molecules in the destabilized motif **VII**, consisting of highly short type I C$_{sp^3}$–F···F–C$_{sp^3}$ interactions (2.663 Å, 132°, 132°), were observed to be stabilized by the presence of water molecules *via* the formation of two strong O$_{water}$–H···O=C hydrogen bonds (motif **II**) in the crystal packing [Fig. 8(a)].

(9) 2-Fluoro-*N*-(4-(trifluoromethyl)phenyl)benzamide (3T1F)

Compound **3T1F** crystallizes in the non-centrosymmetric orthorhombic space group *P*2$_1$*cn* with *Z* = 4. The packing of

molecules in **3T1F** involves the formation of a molecular chain along the *b*-axis with the utilization of strong N–H···O=C along with weak C–H···O=C hydrogen bonds and π···π interactions (motif **I**, −9.7 kcal mol^{-1}, Table S3, ESI†). Such chains are interconnected by the utilization of next two similarly stabilized motifs **II** (−6.5 kcal mol^{-1}) and **III** (−6.3 kcal mol^{-1}) in the formation of a molecular layer down the (101) plane [Fig. 9(a)]. The motif **II** involved a pair of weak C–H···π hydrogen bonds along with short C$_{sp^3}$–F···F–C$_{sp^3}$ (2.840 Å, 127°, 171°) and short C$_{sp^2}$–F···C=O (3.134 Å, 146°) interactions (Table S3, ESI†) whereas a short and directional C–H···π (2.65 Å, 156°) and C–H···F–C$_{sp^3}$ (2.56 Å, 160°) hydrogen bonds were present in motif **III**. Furthermore, a molecular chain formed by the utilization of bifurcated C–H···F–C$_{sp^3}$ hydrogen bonds (motif **IV**, −1.9 kcal mol^{-1}, the 2$_1$ screw parallel to the *a*-axis) was observed to be interconnected *via* motifs **II**, **III** and **V** in the packing of
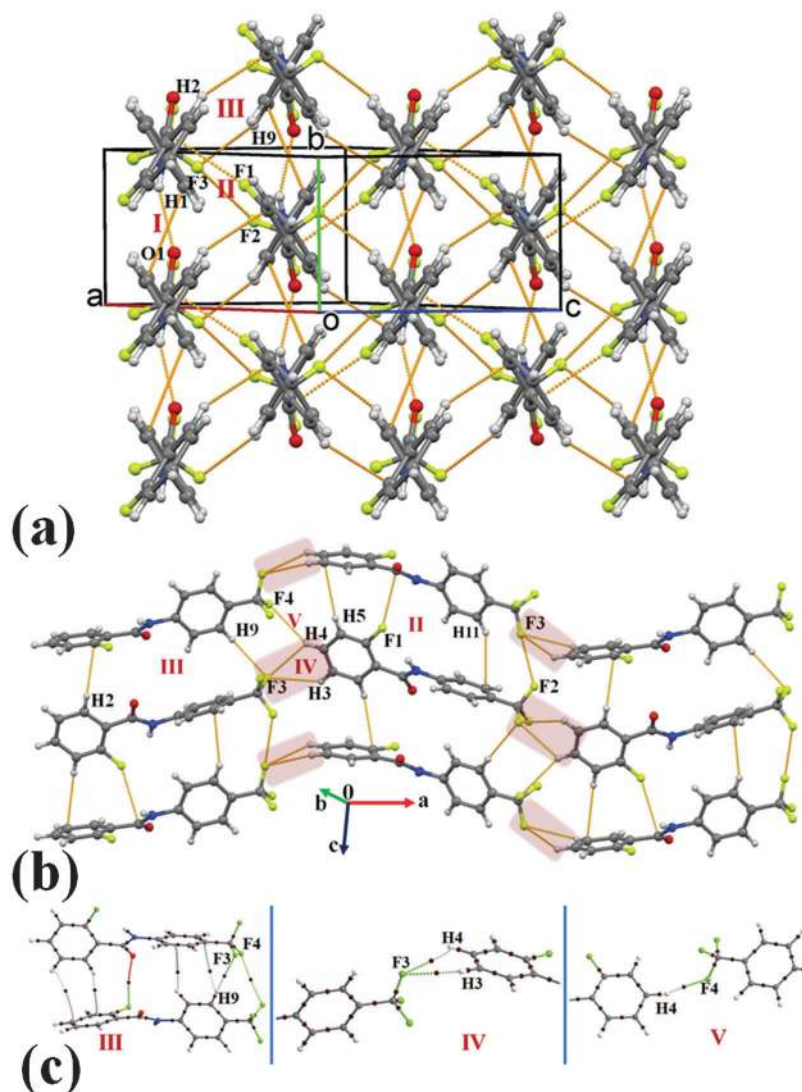
Fig. 9 (a) Packing of molecules in **3T1F** *via* the network of strong N–H···O=C, weak C–H···π, and C–H···F–C$_{sp^3}$ hydrogen bonds along with C$_{sp^3}$–F···F–C$_{sp^3}$, C$_{sp^2}$–F···C=O and π···π interactions. (b) Packing view down the *ac* plane in **3T1F** *via* the network of weak C–H···π and C–H···F–C$_{sp^3}$ hydrogen bonds along with C$_{sp^3}$–F···F–C$_{sp^3}$, C$_{sp^2}$–F···C=O interactions. (c) Selected molecular motifs (Table S4, ESI†) in **3T1F**, showing different intermolecular interactions. Only the interacting part of the motif is shown in the case of **IV–V**.

molecules down the *ac* plane in **3T1F**. The motif **V** (−1.6 kcal mol⁻¹) was found to consist of weak C–H···F–C$_{sp^3}$ hydrogen bonds. These were the presence of (3, −1) BCPs identified in the case of weak C–H···F and C–F···F–C interactions [Fig. 9(c) and Table S4, ESI†].

(10) 3-Fluoro-*N*-(2-(trifluoromethyl)phenyl)benzamide (1T2F)

Compound **1T2F** crystallizes in the centrosymmetric monoclinic space group *P*2₁/*c* with two molecules in the asymmetric unit (*Z* = 8). The two most and similarly stabilized molecular motifs **I** (−12.9 kcal mol⁻¹) and **II** (−12.4 kcal mol⁻¹) were observed to consist of strong N–H···O=C hydrogen bonds along with short C$_{sp^3}$–F···C=O (3.090 Å, 141°; 3.011 Å, 141° respectively, Table S3, ESI†) and π···π interactions. These motifs would appear to be involved in the formation of a ...1212... type molecular chain along the crystallographic *a*-axis. Such chains are recognized to interlink with the exploitation of next four stabilized molecular motifs **III**, **IV**, **V** and **VI**. In the similarly stabilized motifs **III** (−4.6 kcal mol⁻¹) and **IV** (−4.4 kcal mol⁻¹), there were short and directional C–H···O=C (2.33 Å, 149°; 2.23 Å, 168°) hydrogen bonds recognized with the contribution from electrostatic (Coulombic + polarization) being significant (46% and 54% respectively). Further, motifs **V** (involving a bifurcated weak C–H···F–C$_{sp^3}$ and C–H···π hydrogen bonds) and **VI** (involving a bifurcated weak C–H···F–C$_{sp^3}$ hydrogen bond) were observed to provide similar stabilization (−3.5 and −3.2 kcal mol⁻¹ respectively)

to the crystal packing. Moreover, intermolecular interactions involving organic fluorine of type C–H···F, C–F···F–C were noticed to stabilize the crystal packing in **1T2F** and participate in the generation of different supramolecular motifs **VII** to **XII** (Table S3, ESI†) in the crystal packing [Fig. 10(b) and (c)]. The motif **VII** (−2.8 kcal mol⁻¹) was observed to be composed of dimeric weak C–H···F–C$_{sp^3}$ hydrogen bonds along with dimeric C$_{sp^3}$–F···F–C$_{sp^3}$ interactions while a dimeric weak C–H···F–C$_{sp^2}$ hydrogen bond, interacting side wise, was recognized in the equally stabilized motif **VIII**. Further, a bifurcated weak C–H···F–C$_{sp^3}$ hydrogen bond was observed in motif **IX** (−1.8 kcal mol⁻¹) whereas in the similarly stabilized motif **X** (−1.7 kcal mol⁻¹), a short C–H···F–C$_{sp^2}$ hydrogen bond (2.48 Å, 137°) was recognized. In the last two weakly stabilized motifs **XI** (−1.1 kcal mol⁻¹) and **XII** (−0.6 kcal mol⁻¹), a weak C–H···F–C$_{sp^2}$ hydrogen bond and weak type I C$_{sp^3}$–F···F–C$_{sp^2}$ interactions were observed respectively. All the molecular pairs consisting of weak C–H···F and C–F···F–C interactions were analyzed by the theory of QTAIM and the topological parameters were obtained (Table S4, ESI†). There was presence of (3, −1) BCPs noticed for these interactions along with other related contacts in the respective motifs [Fig. 10(d)].

(11) 3-Fluoro-*N*-(3-(trifluoromethyl)phenyl)benzamide (2T2F)

Compound **2T2F** crystallizes in the non-centrosymmetric monoclinic space group *Cc* with four molecules in the unit cell.
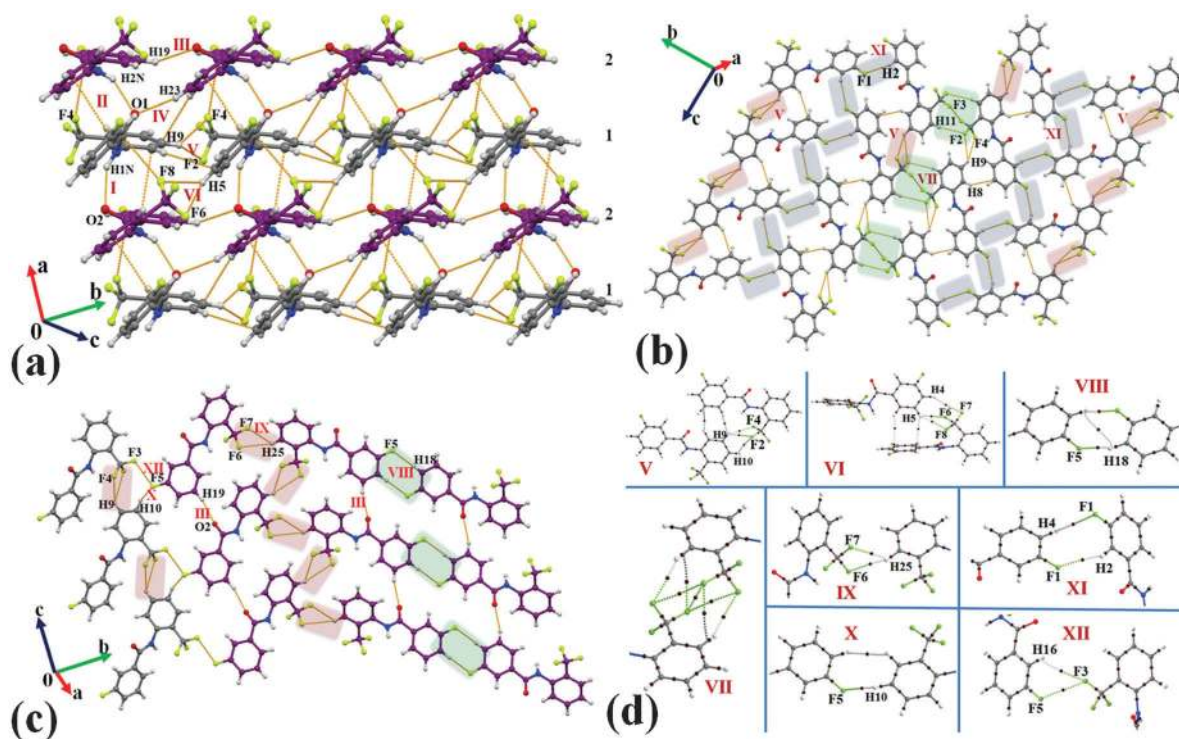
Fig. 10 (a) Formation of the ...1212... type molecular layer in **1T2F** *via* strong N–H···O=C, weak C–H···O, C–H···π, and C–H···F–C$_{sp^3}$ hydrogen bonds along with C$_{sp^3}$–F···C=O and π···π interactions. C-atoms in purple are shown for the second molecule in the asymmetric unit. (b) Packing view down the *bc* plane, displaying the network of weak C–H···π, C–H···F–C$_{sp^2}$, C–H···F–C$_{sp^3}$ hydrogen bonds along with C$_{sp^3}$–F···F–C$_{sp^3}$ interactions in **1T2F**. (c) Packing of molecules in **1T2F** *via* the network of weak C–H···O, C–H···F–C$_{sp^2}$, C–H···F–C$_{sp^3}$ hydrogen bonds along with C$_{sp^3}$–F···F–C$_{sp^3}$ interactions. C-atoms in purple are shown for the second molecule in the asymmetric unit. (d) Selected molecular motifs (Table S4, ESI†) in **1T2F** showing different intermolecular interactions. Only the interacting part of the motif is shown in the case of **VII–XII**.
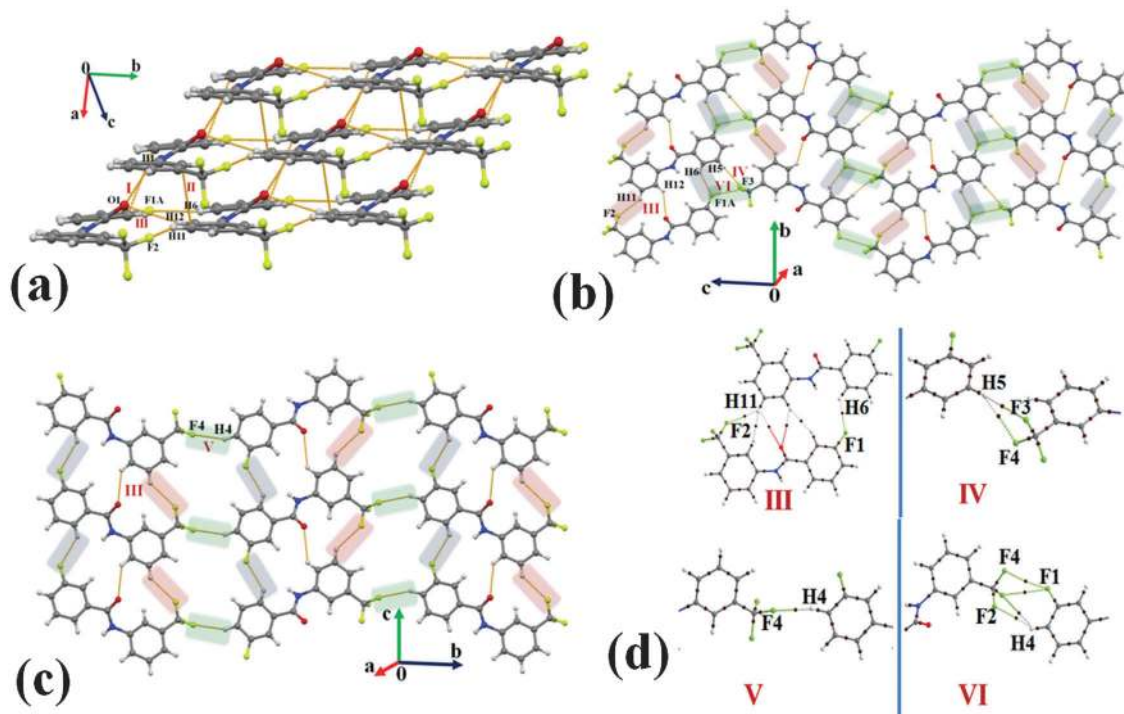
Fig. 11 (a) Packing of molecules in **2T2F** with the utilization of strong N–H···O=C, weak C–H···O, C–H···F–C$_{sp^2}$, and C–H···F–C$_{sp^3}$ hydrogen bonds along with π···π interactions. (b) Formation of a molecular layer down the *bc* plane by the utilization of weak C–H···O, C–H···F–C$_{sp^2}$, and C–H···F–C$_{sp^3}$ hydrogen bonds and C$_{sp^3}$–F···F–C$_{sp^3}$ interactions in **2T2F**. (c) Packing of molecules in **2T2F** *via* weak C–H···O=C, C–H···F–C$_{sp^2}$, and C–H···F–C$_{sp^3}$ hydrogen bonds. (d) Selected molecular motifs (Table S4, ESI†) in **2T2F** showing different intermolecular interactions. Only the interacting part of the motif is shown in the case of **IV–VI**.
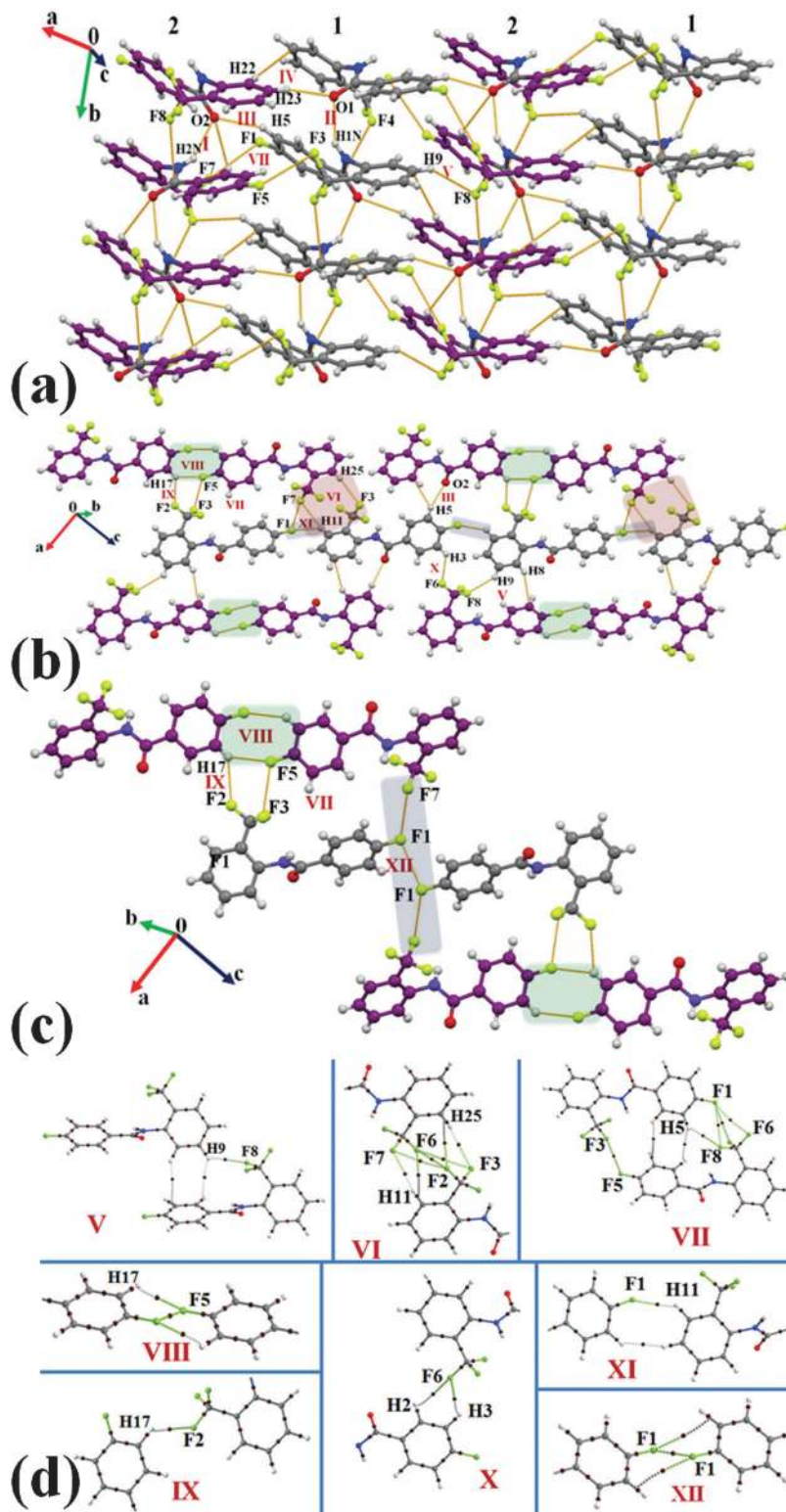
A strong N–H···O=C hydrogen bond along with π···π interactions (motif **I**, −11.3 kcal mol^{-1}) steer the molecules along [110] in the formation of a molecular chain. Such chains are interlinked with the involvement of next two stabilized motifs **II** (−5.5 kcal mol^{-1}) and **III** (−4.8 kcal mol^{-1}) in the crystal packing. The motif **II** was recognized to involve weak π···π interactions with substantial contribution from dispersion energy towards the total stabilization whereas a weak C–H···O=C along with two short C–H···F–C$_{sp^2}$/C$_{sp^3}$ (2.45 Å, 133°; 2.53 Å, 136° respectively) hydrogen bonds were observed in motif **III**. Further the molecular ladder formed *via* the motif **III** was observed to be connected by the utilization of motifs **IV**, **V** and **VI** in the crystal packing [Fig. 11(b) and (c)]. The motif **IV** (−2.2 kcal mol^{-1}) consists of bifurcated weak C–H···F–C$_{sp^3}$ hydrogen bonds while a short C–H···F–C$_{sp^3}$ (2.50 Å, 146°) hydrogen bond was observed in motif **V** (−1.5 kcal mol^{-1}). Moreover, a weak type I C$_{sp^3}$–F···F–C$_{sp^3}$ interaction (motif **VI**, −1.2 kcal mol^{-1}) was also recognized to stabilize the packing of the molecules in **2T2F** (Table S3, ESI†). The presence of (3, −1) BCPs were observed for the weak C–H···F and C–F···F–C interactions in the respective motifs [Fig. 11(d)].

(12) 4-Fluoro-*N*-(2-(trifluoromethyl)phenyl)benzamide (1T3F)

Compound **1T3F** crystallizes in the centrosymmetric monoclinic space group *P*2$_1$/*n* with two molecules in the asymmetric unit (*Z* = 8). The two most stabilized motifs **I** (−12.8 kcal mol^{-1}) and **II** (−12.7 kcal mol^{-1}), involving similar interactions

(strong N–H···O=C hydrogen bonds along with π···π interactions), were observed in the formation of a molecular chain of molecules **1** and **2** in the asymmetric unit, respectively, utilizing *n*-glide along the *b*-axis [Fig. 12(a)]. Such chains are interconnected alternatively with the utilizations of motifs **III**, **IV**, **V** and **VII**. The motifs **III** and **IV** provide similar stabilization (−4.4 kcal mol^{-1} and −4.1 kcal mol^{-1} respectively) and both are involved in the formation of highly short and directional C–H···O=C (2.29 Å, 152°; 2.22 Å, 167° respectively, Table S3, ESI†) hydrogen bonds. A short C–H···F–C$_{sp^3}$ (2.56 Å, 132°) along with a weak C–H···π hydrogen bond were noticed to connect the molecules in motif **V** whereas a near type II along with a near type I C$_{sp^3}$–F···F–C$_{sp^2}$ interactions (2.983 Å, 110°, 165°; 3.128 Å, 90°, 117°) were recognized to stabilize (I.E. being −2.7 kcal mol^{-1}) the crystal packing, existing as motif **VII** (Table S2, ESI†). Further, the packing of molecules in **1T3F** stabilized the formation of two dimeric motifs **VI** (−3.3 kcal mol^{-1}) and **VIII** (−2.1 kcal mol^{-1}) [Fig. 12(b)]. The motif **VI** involved two C–H···F–C$_{sp^3}$ hydrogen bonds along with weak C$_{sp^3}$–F···F–C$_{sp^3}$ interactions (Table S3, ESI†). And the dimeric motif **VIII** was observed to possess short C–H···F–C$_{sp^2}$ (2.48 Å, 131°) hydrogen bonds in the crystal packing in **1T3F**. Moreover, there were three equally stabilized (1.5 kcal mol^{-1}) molecular motifs **IX**, **X** and **XI** observed in the crystal packing and all were noticed to involve weak C–H···F–C hydrogen bonds (Table S2, ESI†). Further a motif (**XII**, −1.3 kcal mol^{-1}), consisting of weak C$_{sp^2}$–F···F–C$_{sp^2}$ interactions and connecting molecules '1' of

Fig. 12 (a) Packing of molecules in **1T3F** *via* the network of strong N−H···O═C, weak C−H···O, C−H···π, and C−H···F−C$_{sp^3/sp^2}$ hydrogen bonds along with C$_{sp^3}$−F···C═O and C$_{sp^3}$−F···F−C$_{sp^2}$ interactions. C-atoms in purple are shown for the second molecule in the asymmetric unit. (b) Formation of the molecular layer down the *ac* plane with the utilization of weak C−H···O═C, C−H···π, C−H···F−C$_{sp^3/sp^2}$ hydrogen bonds along with C$_{sp^3}$−F···F−C$_{sp^2}$ interactions in **1T3F**. (c) Part of crystal packing in **1T3F** showing the presence of weak C−H···F−C$_{sp^3/sp^2}$ hydrogen bonds along with C−F···F−C interactions. (d) Selected molecular motifs (Table S4, ESI†) in **1T3F** showing different intermolecular interactions. Only the interacting part of the motif is shown in the case of **V−XII**.

the asymmetric unit, was observed to stabilize the crystal packing in **1T3F** [Fig. 12(c)]. The weak C–H···F–C hydrogen bonds and C–F···F–C interactions present in the motifs **V** to **XII** in **1T3F** were characterized by the theory of AIM. The presence of (3, −1) BCPs was observed for these interactions [Fig. 12(d)].

### (13) 4-Fluoro-*N*-(4-(trifluoromethyl)phenyl)benzamide (3T3F)

Compound **3T3F** crystallizes in the centrosymmetric monoclinic space group $P2_1/c$ with $Z = 4$. A strong N–H···O=C hydrogen bond, supported by weak C–H···O=C and C–H···π hydrogen bonds (motif **I**, 11.6 kcal mol^{-1}), was observed in the formation of a molecular chain utilizing *c*-glide perpendicular to the *b*-axis in **3T3F** [Fig. 13(a) and (b)]. Such chains are interconnected *via* the motifs **II**, **III**, **V** and **VIII**. The weak π···π interactions were observed to connect molecules in the dimeric motifs **II** (−5.9 kcal mol^{-1}) and **III** (−4.6 kcal mol^{-1}). In the motif **V** (−2.6 kcal mol^{-1}), weak C–H···F–C$_{sp^2}$ hydrogen bonds along with C–H···C=O interactions were recognized whereas a short C–H···F–C$_{sp^3}$ hydrogen bond was observed in motif **VIII** (−1.4 kcal mol^{-1}). The packing of the molecules in **3T3F** involved the formation of a herringbone pattern down the crystallographic *ab* plane with the utilization of motifs **IV** [−2.7 kcal mol^{-1}; involving short C–H···π hydrogen bonds (2.79 Å, 133°; Table S2, ESI†)], **V** and **VIII** [Fig. 13(c)]. Moreover, a bifurcated C–H···F–C$_{sp^2}$ hydrogen bond (motif **VII**, −2.2 kcal mol^{-1}), utilizing *c*-glide, was noticed in the formation of a molecular chain [Fig. 13(d)]. The chain was interlinked *via* the presence of motifs **VI**, **VIII** and **IX**. The motif **VI** (−2.6 kcal mol^{-1}) was found to involve the

weak C–H···F–C$_{sp^3}$ hydrogen bond in the formation of a molecular chain utilizing *c*-glide [Fig. 13(d)]. Dimeric and weakly stabilized (−0.4 kcal mol^{-1}) short C$_{sp^3}$–F···F–C$_{sp^3}$ interactions were identified in the motif **IX**. The molecular motifs **V–VIII** and **IX**, consisting of weak interactions involving fluorine, were studied topologically using the approach of QTAIM. Bond critical points at the bond path for these interactions were observed [Fig. 13(e)].

Therefore, the detailed analysis of all crystal structures revealed that the C(sp^2)/(sp^3)–F group was observed in the formation of different robust structural motifs in the presence of a strong N–H···O=C hydrogen bond and other related weak interactions like C–H···O=C, C–H···π, and π···π. Moreover, in many cases, different supramolecular motifs (Table S3, ESI†) by C(sp^2)/(sp^3)–F from both sides of the molecules can combine co-operatively in the formation of bigger structural motifs in the crystal structures.

Insights from atoms in molecules calculations

It is of interest to conduct topological characterization of H···F and F···F interactions, observed in this class of compounds (including the previously reported crystal structures[17,38–40]) and the analysis of the nature of these interactions along with the relationship of different topological parameters at BCP with bond path length. For this purpose, the selected dimers involving H···F or F···F interactions were identified and QTAIM calculations have been performed at their crystal geometry in accordance with the procedure reported in our earlier work.[41] The results of
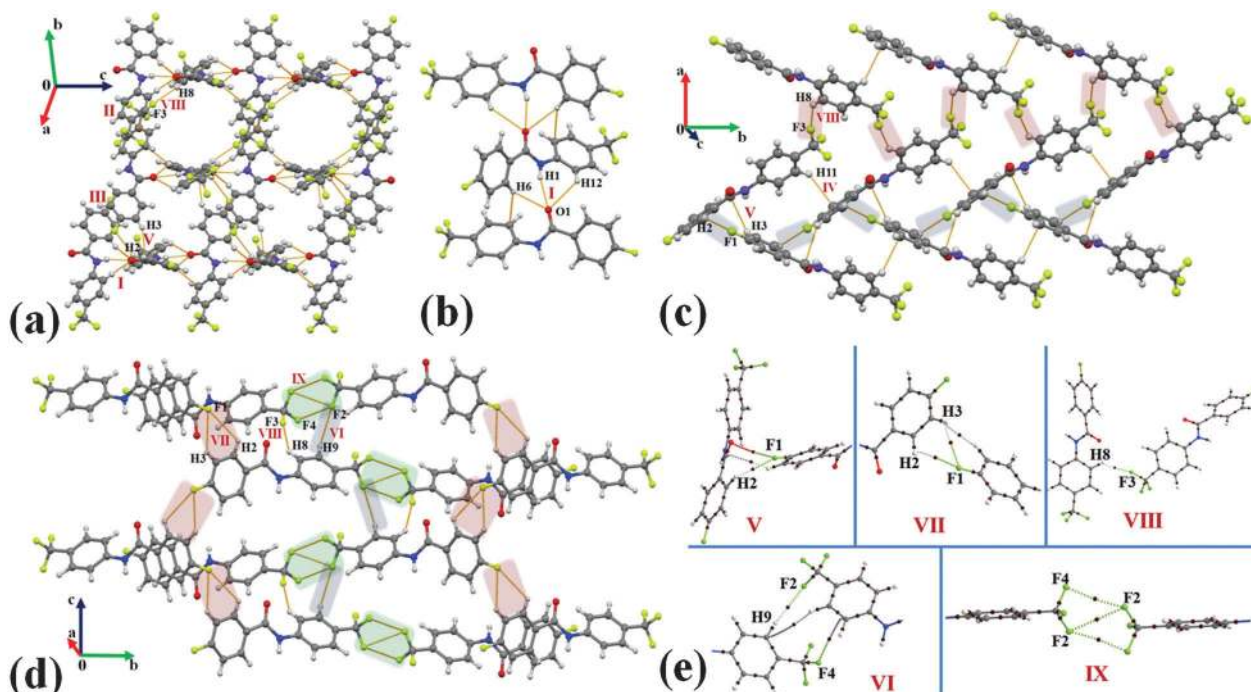
Fig. 13   (a) Packing of molecules in **3T3F** *via* the network of strong N–H···O=C, weak C–H···O, C–H···π, C–H···F–C hydrogen bonds along with π···π interactions. (b) Depiction of a molecular chain *via* the motif **I** in **3T3F**. (c) Formation of a layer down the *ab* plane, utilizing weak C–H···F–C hydrogen bonds and C–H···C=O interactions in **3T3F**. (d) Formation of a weak bifurcated C–H···F–C hydrogen bonds along with C$_{sp^3}$–F···F–C$_{sp^3}$ interactions down the *bc* plane in **3T3F**. (e) Selected molecular motifs (Table S4, ESI†) in **3T3F**, showing different intermolecular interactions. Only the interacting part of the motif is shown in the case of **V–VII** and **IX**.

the calculations are presented in Tables S4 and S5 of Section S4 in the ESI.† Topological parameters of the selected C–H···F and C–F···F–C interactions are given in Table S4b (ESI†).

It is to be noted here that some of the important criteria for an interaction to be called a hydrogen bond or a closed shell type are:[69,70] (i) ρ value at BCP lies within the range [0.013, 0.270] e Å^{-3}, (ii) positive value of the Laplacian of the electron density [$\nabla^2\rho > 0$] indicates closed shell interactions, (iii) the range of Laplacian values [0.578 < $\nabla^2\rho$ (e Å^{-5}) < 3.350] indicates the presence of a "H-bond" and (iv) the value of $|V_b|/G_b < 1$ for hydrogen bonds[71,72] and closed shell interactions; V_b and G_b are the potential and kinetic energy density at BCP. It is of interest to validate the nature of H···F and F···F interactions with these criteria.

Analysis of H···F bonding interactions

H···F interactions were observed to lie in the range of 2.2–3.0 Å for all structures in the current work. As observed earlier,[41] the dependency of electron density (ρ_b) shows exponential dependence with the bond path length (r_{ij}) [Fig. 14(a)] with the values in the range of 0.085 > ρ_b > 0.015 e Å^{-3}. Hence these fulfill the criterion for the interactions to be called a hydrogen bond. The dissociation energy of these interactions (vary exponentially with r_{ij}, [Fig. 14(b)]) were observed between ~3.0 to ~0.4 kcal mol^{-1}. The value of Laplacian observed to be positive [($\nabla^2\rho > 0$), Fig. 14(c)] for the entire bond path length (r_{ij}) suggesting the

closed shell nature of these H···F interactions. It is to be noted that for a short C–H···F bond path length (r_{ij}) at less than the sum of van der Waals radii[73] of H and F, 2.67 Å, the values of the Laplacian are in accordance with the Koch and Popelier criteria for the existence of hydrogen bonds.[74] Moreover, the values of $|V_b|/G_b$ were also observed to be less than one (criteria for hydrogen bonds[71,72]) for the entire range of the bond path [Fig. 14(d)].

Furthermore, it was of interest to study the role of hybridization of the C-atoms to which fluorine is attached in the C–H···F interactions. Hence the variation of dissociation energy (D.E.) (kcal mol^{-1}) and electron density (e Å^{-3}) at the BCP and with H···F bond path length (Å) for C–H···F–C(sp^2) and C–H···F–C(sp^3) has been compared [Fig. 15(a) and (b), Tables S4 and S5, ESI†]. It was observed that the highest stabilized molecular motifs primarily consist of C(sp^2)–H···F–C(sp^2) hydrogen bonds in preference to C(sp^2)–H···F–C(sp^3) hydrogen bonds in the crystal with the difference in energies of stabilization involving fluorine atoms attached to sp^2 and sp^3 carbon is not significant in the molecular crystal [circled area in Fig. 15(a) and (b)].

Analysis of F···F bonding interactions

There are numerous C–F···F–C interactions observed in the crystal packing of this series of compounds (Tables S4 and S5, ESI†). Hence, it was also of interest to do the topological characterization of F···F interactions. The nature and role of C–F···F–C

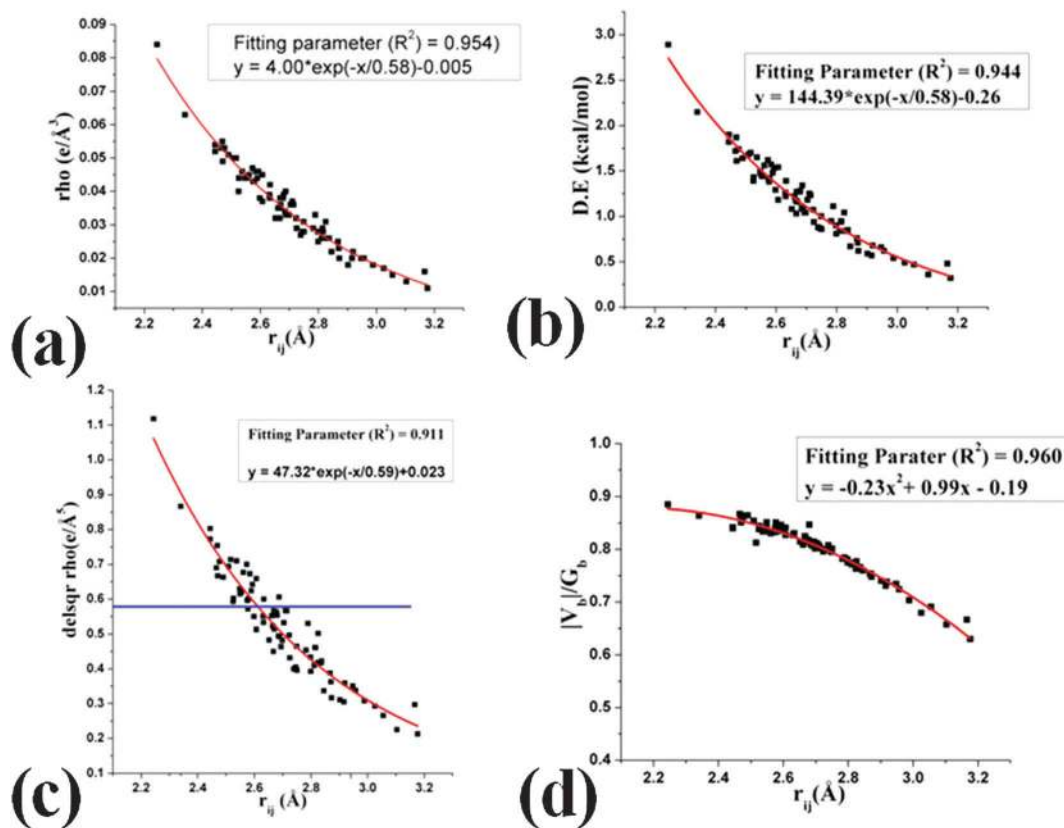**Fig. 14** Variation of (a) electron density (e Å^{-3}) at the BCP, (b) dissociation energy (D.E) (kcal mol^{-1}) with the H···F bond path length (Å), (c) Laplacian ($\nabla^2\rho$) at the BCP and (d) $|V_b|/G_b$ with the H···F bond path length (Å).
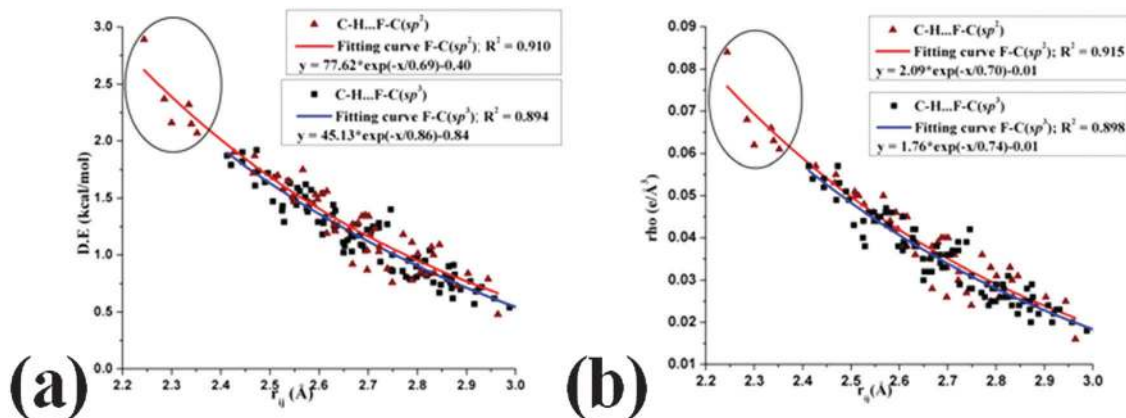
Fig. 15 Comparison of variation of (a) dissociation energy (D.E) (kcal mol^{-1}) and (b) electron density (e Å^{-3}) at the BCP and with the H···F bond path length (Å) for C−H···F−C(sp^2) [red curve] and C−H···F−C(sp^3) [blue curve] [total 153 data points (98 for the red curve and 55 for the blue curve)].

interactions were recently studied both experimentally and theoretically by many researchers.[75,76] The previous report by the QTAIM analysis of intramolecular C−F···F−C interactions on a rigid isolated molecular system showed that these are closed shell interactions and can impart as much as 14 kcal mol^{-1} of local stabilization.[77] In the present work, QTAIM analysis of intermolecular C−F···F−C interactions has been performed and the results show the exponential dependence of electron density at the BCP (ρ_b), dissociation energy (D.E.) and Laplacian ($\nabla^2\rho$) of the electron density at the BCP with the F···F bond path length

(r_{ij}) (Fig. 16). Values of electron density and dissociation energy (local stabilization) were observed between $\sim 0.060 > \rho_b$ (e Å^{-3}) $> \sim 0.010$ and $\sim 2.8 <$ D.E. (kcal mol^{-1}) $< \sim 0.5$ for the $\sim 2.80 > r_{ij}$ (Å) > 3.45. These values are slightly less or comparable with weak C−H···F−C interactions in the present work and observed to be similar to the previously observed values.[67,77–80] Furthermore, for the entire range of the F···F bond path length, Laplacian values ($\nabla^2\rho$) > 1 and $|V_b|/G_b < 1$ were observed. Hence it can be concluded that the intermolecular F···F interactions in the present work are of closed shell in nature. Furthermore, the nature

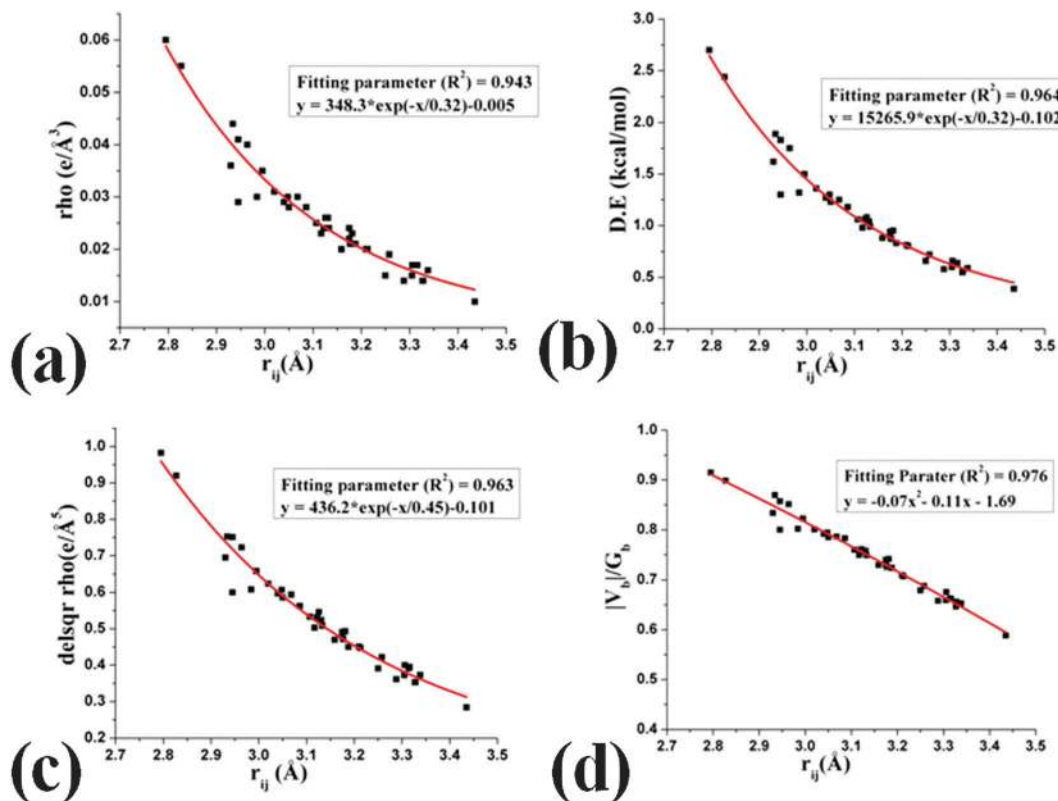**Fig. 16** Variation of (a) electron density (e Å^{-3}), (b) dissociation energy (D.E) (kcal mol^{-1}) with the F···F bond path length (Å) [42 data points], (c) Laplacian ($\nabla^2\rho$) at the BCP and (d) $|V_b|/G_b$ with the F···F bond path length (Å).

Table 1 Topological parameters from previous reports on C–F···F–C interactions by charge density analysis of high resolution X-ray data

| Nature of interactions	R_{ij} (Å)	ρ (e Å^{-3})	$\nabla^2\rho$ (e Å^{-5})	Ref.
C(sp^2)–F···F–C(sp^2); type I	2.8091	0.049	1.030	78
C(sp^2)–F···F–C(sp^2); type I	2.8187	0.040	0.820	79
C(sp^2)–F···F–C(sp^2); type II	2.8240	0.040	0.900	80
C(sp^3)–F···F–C(sp^3); type II	2.9255	0.030	0.633	67
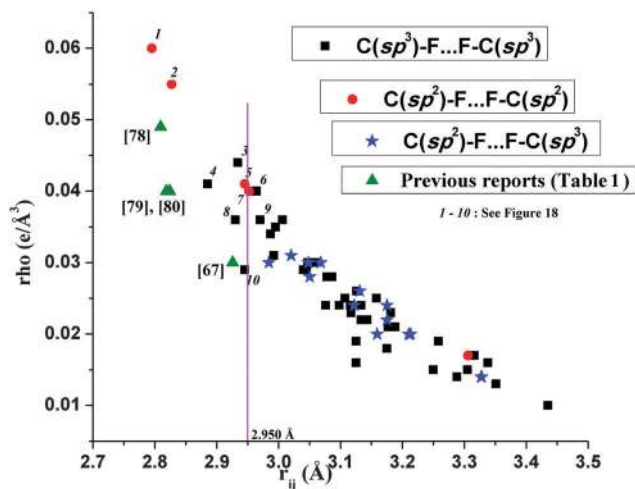
Fig. 17 Comparison of the variation of the electron density (e Å^{-3}) at the BCP and with the F···F bond path length (Å) for C(sp^3)/(sp^2)–F···F–C(sp^3)/(sp^2) interactions from current and previous studies [total 64 data points].

of C(sp^3)/(sp^2)–F···F–C(sp^3)/(sp^2) interactions from current and previous studies along with reports from experimental charge density analysis (Table 1) have been compared in Fig. 17. The results show the small differences in the ρ_b (e Å^{-3}) at the BCP for different types of C–F···F–C interactions involving fluorine atoms attached to sp^2 and sp^3 carbon atoms. The shorter C–F···F–C interactions were observed to be associated with the C(sp^2)–F bond in the molecule in the crystal. It is also of interest to notice variations in ρ_b, dissociation energy (D.E.) and Laplacian ($\nabla^2\rho$) of the electron density at the BCP for a given value of r_{ij}. Different values of electron density at the BCP for C(sp^3)/(sp^2)–F···F–C(sp^3)/(sp^2) interactions for the nearly same r_{ij} (A) of the F···F bond path (near to the sum of van der Waals radii of the F-atom, 2.94 A) in the case of 3, 5, 6, 7, 8, 10 have been observed [Fig. 18]. This feature may be explained due to the cooperative interplay amongst the different possible intermolecular bond paths present in the motifs 3, 5, 6, 7 and 8 whereas in the case of 10 (having the least value of ρ_b among these), only one C(sp^3)–F···F–C(sp^3) is present.

Conclusion

Following the analysis of the 15 crystal structures (including one hydrate) from the 18 newly synthesized compounds along with the inputs from previously reported structures, the role of organic fluorine in the crystal packing has been analyzed in the presence of strong hydrogen bonds. The formation of many "reoccurring" structural motifs by the C$_{sp^2}$–F and CF$_3$ group has been identified and investigated in terms of their nature, energetics and topological properties, which were quantified by the PIXEL method and the QTAIM approach. It was observed that the highest stabilized molecular motifs primarily consist of C(sp^2)–H···F–C(sp^2) hydrogen bonds in preference to C(sp^2)–H···F–C(sp^3) H bonds in the crystal. Moreover, the formation of hydrogen bonds by the C(sp^2)/(sp^3)–F group was observed to be present over the entire distance range between 2.2 and 2.7 Å (from the QTAIM approach), albeit the difference in energies of stabilization involving fluorine atoms attached to
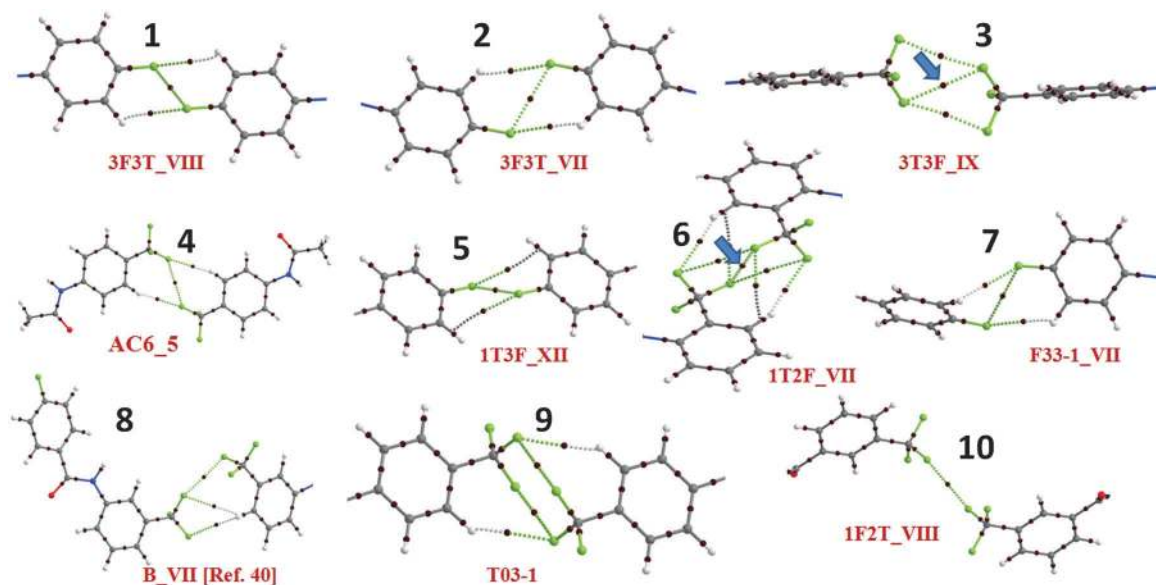
Fig. 18 Showing first ten more stabilized motifs in Fig. 17, having C(sp^3)/(sp^2)–F···F–C(sp^3)/(sp^2) interactions near or below the sum of van der Waals radii of two F-atoms, 2.94 Å.

sp^2 and sp^3 carbon is not of significance in molecular crystals. Following the analysis of $C(sp^2)/(sp^3)$–$F\cdots F$–$C(sp^2)/(sp^3)$ interactions from the QTAIM approach, it was observed that these fulfill the criteria of these being of the closed shell type for the entire $F\cdots F$ bond path length and provide local stabilization (indicates the formation of bonds) similar to the case of weak hydrogen bonds in crystals. For future study, it would be of interest to extend this study to donor atoms in different hybridization environments with the F–$C(sp^2)/(sp^3)$ group in different chemical environments. Furthermore, it is also of interest to investigate the effect of increasing fluorination on the molecule and the impact on the stabilization energies for the different supramolecular motifs involving organic fluorine present in the crystal.

Acknowledgements

References

1 H.-J. Schneider, *Chem. Sci.*, 2012, **3**, 1381–1394.

2 G. K. S. Prakash, F. Wang, M. Rahm, J. Shen, C. Ni, R. Haiges and G. A. Olah, *Angew. Chem., Int. Ed.*, 2011, **50**, 11761–11764.

3 F. F. Awwadi, R. D. Willett, K. A. Peterson and B. Twamley, *Chem. – Eur. J.*, 2006, **12**, 8952.

4 M. Perez-Torralba, M. A. Garcia, C. Lopez, M. C. Torralba, M. R. Torres, R. M. Claramunt and J. Elguer, *Cryst. Growth Des.*, 2014, **14**, 3499–3509.

5 I. Saraogi, V. G. Vijay, S. Das, K. Sekar and T. N. G. Row, *Cryst. Eng.*, 2003, **6**, 69–77.

6 M. T. Scerba, S. Bloom, N. Haselton, M. Siegler, J. Jaffe and T. Lectka, *J. Org. Chem.*, 2012, **77**, 1605–1609.

7 X. Xu, B. Pooi, H. Hirao and S. H. Hong, *Angew. Chem., Int. Ed.*, 2014, **53**, 1283–1287.

8 R. Berger, G. Resnati, P. Metrangolo, E. Weber and J. Hulliger, *Chem. Soc. Rev.*, 2011, **40**, 3496–3508 and references therein.

9 L. Shimoni and J. P. Glusker, *Struct. Chem.*, 1994, **5**, 383–397.

10 J. A. K. Howard, V. J. Hoy, D. O'Hagan and G. T. Smith, *Tetrahedron*, 1996, **52**, 12613–12622.

11 J. D. Dunitz and R. Taylor, *Chem. – Eur. J.*, 1997, **3**, 89–98.

12 V. R. Thalladi, H.-C. Weiss, D. Blaser, R. Boese, A. Nangia and G. R. Desiraju, *J. Am. Chem. Soc.*, 1998, **120**, 8702–8710.

13 J. Parsch and J. W. Engels, *J. Am. Chem. Soc.*, 2002, **124**, 5564–5572.

14 J. D. Dunitz, *ChemBioChem*, 2004, **5**, 614–621.

15 J. D. Dunitz and W. B. Schweizer, *Chem. – Eur. J.*, 2006, **12**, 6804–6815.

16 F. Cozzi, S. Bacchi, G. Filippini, T. Pilati and A. Gavezzotti, *Chem. – Eur. J.*, 2007, **13**, 7177–7184.

17 D. Chopra and T. N. G. Row, *CrystEngComm*, 2008, **10**, 54–67.

18 T. S. Thakur, M. T. Kirchner, D. Blaser, R. Boese and G. R. Desiraju, *CrystEngComm*, 2010, **12**, 2079–2085.

19 K. Muller, C. Faeh and F. Diederich, *Science*, 2007, **317**, 1881–1886.

20 D. Chopra and T. N. G. Row, *CrystEngComm*, 2011, **13**, 2175–2186 and references therein.

21 D. Chopra, *Cryst. Growth Des.*, 2012, **12**, 541–546 and references therein.

22 P. A. Champagne, J. Desroches and J.-F. Paquin, *Synthesis*, 2015, 306–322 and references therein.

23 P. Panini and D. Chopra, in *Hydrogen Bonded Supramolecular Structures*, ed. Z. Li and L. Wu, Lecture Notes in Chemistry, Springer-Verlag, Berlin, Heidelberg, 2015, vol. 87, pp. 37–67, ISBN: 978-3-662-45755-9.

24 A. R. Choudhury and T. N. G. Row, *Cryst. Growth Des.*, 2004, **4**, 47–52.

25 A. R. Choudhury and T. N. G. Row, *CrystEngComm*, 2006, **8**, 265–274.

26 D. Chopra, V. Thiruvenkatam, S. G. Manjunath and T. N. G. Row, *Cryst. Growth Des.*, 2007, **7**, 868–874.

27 A. Schwarzer and E. Weber, *Cryst. Growth Des.*, 2008, **8**, 2862–2874.

28 V. Vasylyeva and K. Merz, *Cryst. Growth Des.*, 2010, **10**, 4250–4255.

29 V. Vasylyeva, O. V. Shishkin, A. V. Maleev and K. Merz, *Cryst. Growth Des.*, 2012, **12**, 1032–1039.

30 M. Karanam and A. R. Choudhury, *Cryst. Growth Des.*, 2012, **13**, 4803–4814.

31 G. Kaur, P. Panini, D. Chopra and A. R. Choudhury, *Cryst. Growth Des.*, 2012, **12**, 5096–5110.

32 G. Kaur and A. R. Choudhury, *Cryst. Growth Des.*, 2014, **14**, 1600–1616.

33 K. Merz, M. V. Evers, F. Uhl, R. I. Zubatyuk and O. V. Shishkin, *Cryst. Growth Des.*, 2014, **14**, 3124–3130.

34 P. Panini and D. Chopra, *New J. Chem.*, 2015, **39**, 8720–8738.

35 A. Abad, C. Agullo, A. C. Cunat, C. Vilanova and M. C. R. de Arellano, *Cryst. Growth Des.*, 2006, **6**, 46–57.

36 P. Mocilac, K. Donnelly and J. F. Gallagher, *Acta Crystallogr., Sect. B: Struct. Sci.*, 2012, **68**, 189–203.

37 R. Dubey, M. S. Pavan and G. R. Desiraju, *Chem. Commun.*, 2012, **48**, 9020–9022.

38 M. Perez-Torralba, M. A. Garcia, C. Lopez, M. C. Torralba, M. R. Torres, R. M. Claramunt and J. Elguer, *Cryst. Growth Des.*, 2014, **14**, 3499–3509.

39 P. Panini and D. Chopra, *CrystEngComm*, 2013, **15**, 3711–3733.

40 P. Panini and D. Chopra, *CrystEngComm*, 2012, **14**, 1972–1989.

41 P. Panini and D. Chopra, *Cryst. Growth Des.*, 2014, **14**, 3155–3168.

42 R. F. W. Bader, *Atoms in Molecules: A Quantum Theory*, Oxford University Press, Oxford, UK, 1990.

43 (*a*) E. Arunan, G. R. Desiraju, R. A. Klein, J. Sadlej, S. Scheiner, I. Alkorta, D. C. Clary, R. H. Crabtree, J. J. Dannenberg, P. Hobza, H. G. Kjaeergaard, A. C. Legon, B. Mennucci and D. J. Nesbitt, *Pure Appl. Chem.*, 2011, **83**, 1619–1636; (*b*) E. Arunan, G. R. Desiraju, R. A. Klein, J. Sadlej, S. Scheiner, I. Alkorta, D. C. Clary, R. H. Crabtree, J. J. Dannenberg,

P. Hobza, H. G. Kjaeergaard, A. C. Legon, B. Mennucci and D. J. Nesbitt, *Pure Appl. Chem.*, 2011, **83**, 1637–1641.

44 A. Gavezzotti, *New J. Chem.*, 2011, **35**, 1360–1368.

45 A. Gavezzotti, *Mol. Phys.*, 2008, **106**, 1473–1485.

46 L. Maschio, B. Civalleri, P. Ugliengo and A. Gavezzotti, *J. Phys. Chem. A*, 2011, **115**, 11179–11186.

47 J. D. Dunitz and A. Gavezzotti, *Cryst. Growth Des.*, 2012, **12**, 5873–5877.

48 R. Shukla and D. Chopra, *CrystEngComm*, 2015, **17**, 3596–3609.

49 V. Petricek, M. Dusek and L. Palatinus, *JANA 2000*, 18/12/2007, Institute of Physics, Czech Republic, 2007, http://jana.fzu.cz.

50 A. Altomare, G. Cascarano, C. Giacovazzo and A. Guagliardi, *J. Appl. Crystallogr.*, 1993, **26**, 343–350.

51 G. M. Sheldrick, *Acta Crystallogr., Sect. A: Found. Crystallogr.*, 2008, **64**, 112–122.

52 L. J. Farrugia, WinGX, *J. Appl. Crystallogr.*, 1999, **32**, 837–838.

53 C. F. Macrae, I. J. Bruno, J. A. Chisholm, P. R. Edgington, P. McCabe, E. Pidcock, L. Rodriguez-Monge, R. Taylor, J. Streek and P. A. Wood, *J. Appl. Crystallogr.*, 2008, **41**, 466–470www.ccdc.cam.ac.uk/mercury.

54 P. Panini, K. N. Venugopala, B. Odhav and D. Chopra, *Acta Crystallogr., Sect. B: Struct. Sci., Cryst. Eng. Mater.*, 2014, **70**, 681–696.

55 R. Shukla, T. P. Mohan, B. Vishalakshi and D. Chopra, *CrystEngComm*, 2014, **16**, 1702–1713.

56 D. Dey, T. P. Mohan, B. Vishalakshi and D. Chopra, *Cryst. Growth Des.*, 2014, **14**, 5881–5896.

57 P. Panini, R. Shukla, T. P. Mohan, B. Vishalakshi and D. Chopra, *J. Chem. Sci.*, 2014, **126**, 1337–1345.

58 S. Grimme, J. Antony, S. Ehrlich and H. Krieg, *J. Chem. Phys.*, 2010, **132**, 154104.

59 W. Hujo and S. Grimme, *Phys. Chem. Chem. Phys.*, 2011, **13**, 13942–13950.

60 R. Ahlrichs, M. Baer, M. Haeser, H. Horn and C. Koelmel, Electronic structure calculations on work-station computers: the program system TURBOMOLE, *Chem. Phys. Lett.*, 1989, **162**, 165–169.

61 F. Bernardi and S. F. Boys, *Mol. Phys.*, 1970, **19**, 553.

62 T. A. Keith, *AIMALL, version 13.05.06*, TK Gristmill Software, Overland Park KS, USA, 2013, aim.tkgristmill.com.

63 E. Espinosa, E. Molins and C. Lecomte, *Chem. Phys. Lett.*, 1998, **285**, 170–173.

64 I. Mata, I. Alkorta, E. Espinosa and E. Molins, *Chem. Phys. Lett.*, 2011, **507**, 185–189.

65 M. V. Vener, A. N. Egorova, A. V. Churakov and V. G. Tsirelson, *J. Comput. Chem.*, 2012, **33**, 2303–2309.

66 E. D'Oria and J. J. Novoa, *CrystEngComm*, 2008, **10**, 423–436.

67 V. R. Hathwar, D. Chopra, P. Panini and T. N. G. Row, *Cryst. Growth Des.*, 2014, **14**, 5366–5369.

68 R. M. Osuna, V. Hernàndez, J. T. L. Navarrete, E. D'Oria and J. J. Novoa, *Theor. Chem. Acc.*, 2011, **128**, 541–553.

69 P. L. Popelier, *Atoms in Molecules: An Introduction*, Prentice Hall, London, 2000.

70 U. Koch and P. L. A. Popelier, *J. Phys. Chem.*, 1995, **99**, 9747–9754.

71 I. Mata, I. Alkorta, E. Molins and E. Espinosa, *Chem. – Eur. J.*, 2010, **16**, 2442–2452.

72 E. Espinosa, I. Alkorta, J. Elguero and E. Molins, *J. Chem. Phys.*, 2002, **117**, 5529–5542.

73 A. Bondi, *J. Phys. Chem.*, 1964, **68**, 441–451.

74 G. Zhang, W. He and D. Chen, *Mol. Phys.*, 2014, **112**, 1736–1744.

75 R. J. Baker, P. E. Colavita, D. M. Murphy, J. A. Platts and J. D. Wallis, *J. Phys. Chem. A*, 2012, **116**, 1435–1444.

76 R. A. Cormanich, R. Rittner, D. O'Hagan and M. Bühl, *J. Phys. Chem. A*, 2014, **118**, 7901–7910.

77 C. F. Matta, N. Castillo and R. J. Boyd, *J. Phys. Chem. A*, 2005, **109**, 3669–3681.

78 D. Chopra, T. S. Cameron, J. D. Ferrara and T. N. G. Row, *J. Phys. Chem. A*, 2006, **110**, 10465–10477.

79 V. R. Hathwar and T. N. G. Row, *Cryst. Growth Des.*, 2011, **11**, 1338–1346.

80 M. S. Pavan, K. D. Prasad and T. N. G. Row, *Chem. Commun.*, 2013, **49**, 7558–7560.